

POLITECNICO DI TORINO

Master of science in “Nanotechnologies for ICTs”

Master’s degree thesis



**A new xenograft *in ovo* model to study the effects of
gold nanoparticles radiotherapy to treat lung cancer**

Supervisors:

Prof. Matteo Cocuzza
Dott. Giancarlo Canavese
Prof. Alessandro Grattoni

Candidate:

Francesca Ferraro

April 2018

*Ai miei genitori,
che mi hanno sempre permesso di scegliere il meglio*

Abstract

Cancer is still a worldwide problem that induces the constant need of new solutions for studying possible treatments at research level. Radiotherapy is one of the mostly used approach to fight against cancer, with a big drawback: the radiation is incapable to distinguish between healthy and cancer cells, so it is an invasive therapy. The use of radioenhancers has been investigated during the last decades as one of the possibility to be able to lower the general delivered radiation dose and, in particular, gold nanoparticles (GNP) have been the main candidates for this purpose due to the fact that they are inert biocompatible materials and have very low toxicity. This thesis focuses on the demonstration of the radioenhancement capabilities of unfuctionalized GNP on Lewis lung cells derived tumors. The work evolves from *in vitro* to *in vivo* experiments, however, as an alternative to the commonly used mouse model, we present a new alternative model: the chick chorioallantoic membrane (CAM). Being immunodeficient, fecundated chicken eggs can host, on their CAM, any type of cells, resulting in an ideal environment for tumor growth due to the presence of a blood vessel network that can aliment the carcinoma. To the best of our knowledge we were the first to irradiate chicken eggs affected with Lewis lung cell derived tumors and, for this reason, several preliminary experiments were done in order to optimize the number of cells, the amount of gold nanoparticles and the radiation doses, using IVIS imaging as diagnostic tool to monitor tumor growth/reduction. To validate the results of the *in ovo* experiments, similar experiments were performed with C657Bl/6 mice.

Our work is highly relevant as it verifies that the CAM is a robust and efficient model to obtain preliminary data on the synergistic effect of gold nanoparticles and x-ray radiation. We believe that our work will translate to lower radiation doses required in the clinic, improving patient outcomes through less invasive treatment, faster recovery, and reduced damage to healthy tissue.

Acknowledgments

First of all I would like to thank the people that directly helped me for the development of this thesis: ALL the Grattoni's lab of the Houston Methodist Research Institute, Dr. Ravi Pathak, Dr. Arvind Pandey and the researchers of their laboratories.

In particular thanks to Prof. Alessandro Grattoni that gave me the opportunity to join his lab and that believed so much in me.

Thanks to Giacomo that helped me in all the steps (a lot!) that are needed to finally reach Houston and thanks to all his suggestions.

Thanks to Giovanni, Marco, Corrine for all the very helpful talks about my future (PhD or no PhD??).

Thanks to Nicola, Veronica, Maria and Nicola for having established our little IMT italian community.

Thanks to Sid and all the "barbecue crew" for all the trips and talks.

Thanks again to Veronica and Nicola because they will continue the work I started.

Last but not least a very big thanks to Carly! You have been a very patient teacher and thanks to you I have learned soooo much. You gave me the opportunity to grow and learn what it means to do science!

Questa tesi conclude il mio percorso universitario durante il quale ho avuto la possibilità di incontrare tantissime persone speciali e a cui rivolgo i miei sentiti ringraziamenti.

Grazie a Ema, Gianna e Jessica per il bellissimo e divertente periodo passato insieme.

Grazie a tutti i componenti del gruppo "Forno e Pannocchia" (Davide, Federico, Giuseppe, Marco, Tiziano e Valentina) perchè senza di voi questi due anni di specialistica sarebbero stati mooolto più noiosi.

Un grazie alla "Società" per avermi sempre sostenuta (non solo in questi anni universitari) e per aver condiviso tutti i piccoli passi della vita.

GRAZIE alla mia famiglia e a Francesco perchè senza di loro non ce l'avrei mai fatta.

Contents

1	Introduction: state of the art and objectives	3
1.1	Radiotherapy and radioenhancers	3
1.2	An alternative to conventional animal models: the CAM	4
1.3	Research objectives	5
2	Physics of radioenhancement of metal nanoparticles	6
2.1	Introduction	6
2.2	Photoelectric and Auger effects	6
2.3	The Local Effect Model and its limitations	7
3	Materials and methods	10
3.1	Gold nanoparticles	10
3.1.1	Synthesis	10
3.1.2	Characterization	11
3.2	Lewis Lung Cells	17
3.2.1	Cells splitting, counting and cryo-conservation	17
3.2.2	LLC Luciferase gene expressing	19
3.3	CAM model	19
3.3.1	Opening the egg	19
3.3.2	Inoculation of cells and tumor growth	20
3.3.3	Gold nanoparticles on CAM	21
3.3.4	Tumor harvesting and histology	21
3.4	Radiation equipment	22
3.5	Bioluminescence and IVIS imaging	25
4	Experiments design	27
4.1	<i>In vitro</i> experiments	27
4.1.1	Evaluation of growth rate of Lewis Lung Cells luciferase expressing	27
4.1.2	Cellular uptake <i>in vitro</i> study	28
4.1.3	<i>In vitro</i> radiation experiments	28

4.2	<i>In ovo</i> experiments	30
4.2.1	Preliminary experiment: optimization of the initial number of cell . .	31
4.2.2	Preliminary experiment: optimization of the amount of gold in the eggs	31
4.2.3	Preliminary experiment: optimization of X-ray dose for eggs	32
4.2.4	Synergistic effect of gold nanoparticles and radiation	33
4.3	<i>In vivo</i> experiments	34
4.3.1	Preliminary experiment: optimization of radiation dose	34
4.3.2	<i>In vivo</i> GNP radioenhancement	36
5	Results and discussion	37
5.1	Nanoparticles characterization: results and images	37
5.2	<i>In vitro</i> experiments results	39
5.2.1	Evaluation of growth rate of Lewis Lung Cells luciferase expressing	39
5.2.2	Cellular uptake experiment	39
5.2.3	Comet assay and clonogenic assay	41
5.3	<i>In ovo</i> experiments results	43
5.3.1	Preliminary experiment: optimization of the initial number of cell . .	43
5.3.2	Preliminary experiment: optimization of the amount of gold in the eggs and GNP detection	45
5.3.3	Preliminary experiment: optimization of the X-ray dose for the eggs	48
5.3.4	Synergistic effect of gold nanoparticles and radiation	48
5.4	<i>In vivo</i> experiments results	55
5.4.1	Preliminary experiment: optimization of radiation dose	55
5.4.2	<i>In vivo</i> GNP radioenhancement	56
6	Conclusions, improvements and future work	59
	Bibliography	61

Chapter 1

Introduction: state of the art and objectives

1.1 Radiotherapy and radioenhancers

Cancer is still a worldwide problem and the second cause of death in the United States according to the *American Cancer Society* statistics (year 2017) [1]. Different types of treatment exist and often they are used in combination, depending on the stage and type of tumor. The most important are surgery, systemic therapies (like chemotherapy) and radiation therapy. It is well known that radiations cause cells death without discriminate between healthy and cancer cells. That's why there is the need of using radioenhancers that allow to lower the general delivered dose, still having a significant action where the radioenhancer is present. If delivered to the tumor, metallic nanoparticles can locally enhance the radiation, working as *in situ* amplifiers of the action of X-rays, damaging nearby tumor cells. The physical process will be analyzed in Chapter 2. In particular gold nanoparticles have been studied worldwide for this application. The principal reason is that gold is an inert material and it is biocompatible. However, the potentiality and the efficacy of GNPs as radioenhancer depends on a lot of factors. In their review paper S. Shrestha *et al.* give an exhaustive overview among all the parameters that a researcher has to take into account in these type of study [2]. One of the most important factor is the *in situ* delivery of GNP. In order to be effective the particle has to be in close proximity with the tumor cells. Several *in vivo* studies have been done (mouse model) to understand the biodistribution of non functionalized GNP when injected in the tail vein. In these cases the so called enhanced permeation and retention (EPR) effect is exploited, i.e. the natural tendency of particles to localize in the tumor proximity due to their size and to the peculiar cancer vascularization. However it is demonstrated that a great percentage of gold

injected goes in the so called target organs and in particular in the spleens [3]. That's why it is preferable an intratumoral injection of GNP that, on the other hand, can be limited for the superficial tumors. It is interesting to notice that unfunctionalized GNP can be internalized in cancer cells resulting in a more effective treatment and their uptake probability depends on the size and shape of the particles. Chithrani *et al.* demonstrate that the optimal condition is for spherical nanoparticles with a diameter of 50 nm [4], [3].

1.2 An alternative to conventional animal models: the CAM

All the before cited studies from the literature have been performed *in vitro* and *in vivo* and exploit the mouse model as an opportunity to do cancer research. However there exists a less common xenograft model: the chick chorioallantoic membrane (CAM). The CAM is a membrane that starts to develop in the fecundated chicken egg from day 7 after fertilization [5] and works as the respiratory system of the chicken embryo. The lack of an immune system and the high vascularization result in an ideal environment for tumor growth starting from any kind of tumor cells. Dr. Ravi Pathak and his team, with which I had the honour to collaborate, explain in their paper the technique that allows to inoculate cells on the CAM [5]. I will enter more in details on this in the Chapter 3 of this thesis. Nowadays the CAM model is successfully used in laboratory for the study of drug response of tumors xenografted from patients with the aim to develop personalized therapies according to the needs of each medical case, or to analyze the response to particular drugs to, for example, optimize the dose. Other options are the opportunity to study the vascularization of cancers, angiogenesis, metastasis development [6], but also tissue engineering [7].

One of the great advantages of this model that the cited papers underline is the "speed" of the chicken embryo biological system. In other words the studies on tumors can be faster than the ones on mice, since the tumor can reach reasonable dimensions in few days after cell inoculation. Another advantage is the cost of purchasing and maintenance of an egg with respect a mouse, nearly 10 times lower. Furthermore, there is no need to generate an Institutional Animal Care and Use Committee (IACUC) or similar protocol, since, until day 14, the embryo is not considered an animal.

1.3 Research objectives

The objective of this study is to demonstrate that the CAM can be used for radiation studies resulting in a less expensive and faster research opportunity. To the best of our knowledge our group has been the first to investigate this opportunity, and the first to inject GNP on the CAM for radiosensitization experiments. For this reasons several radiation optimizing experiments have been performed in order to understand the right radiation dose for this system. The cell line under investigation is the Lewis Lung, highly tumorigenic for C57B1 mice. To validate our research, mice experiments have been done and the results compared. The idea was also to exploit gold nanoparticles of two different diameters to analyze the possible different effectivenesses according to the size and consequently different uptake percentages of the cells. Unfortunately, due to lack of time, this was not possible. However, in this thesis, the synthesis and characterization of GNP of both sizes will be reported.

Chapter 2

Physics of radioenhancement of metal nanoparticles

2.1 Introduction

In this chapter I want to briefly describe the physical process beyond radiosensitization of metal nanoparticles and its possible modellization. The main event occurring in the process is the photoelectric effect. After irradiation, in fact, the metal particle will produce photoelectrons followed by Auger electrons and characteristic X-rays that should release their energy at the nearby cells. What is not completely clear is the biological process that brings the cell to death. This, in fact, involves a series of phenomena that result in a dependence of the outcomes on the cell type, its behavior and the received dose.

Harold N. McQuaid *et al.*[8] try to give a general view of the phenomenon comparing the known Local Effect Model (LEM) with a developed biophysical model that takes into account the distance of the particles from the cell, the amount of DNA damage, the energy and the dose deposition.

2.2 Photoelectric and Auger effects

After the interaction of a material with radiation, several events can occur with a certain probability: emission of another electron (photoelectron), emission of an Auger electron or characteristic X-ray emission. Let's briefly analyze the three phenomena considering just an atom and its energy levels.

Consider an electron in the inner core of the atom. If the energy of the incoming photon is at least equal to the binding energy of the electron, it can take this energy and escape from

the material overcoming the vacuum level. Its final energy will depend on the incoming photon one:

$$E_f = h\nu - E_B \quad (2.1)$$

where h is the Planck's constant, ν is the frequency of the incoming photon and E_B is the binding energy.

The photoelectron will leave a hole in the inner energy level of the atom (ionizing event) that will be filled by one of the electrons in the outer shell (relaxation process). The excess energy can be released by emission of characteristic X-ray radiation or by emission of an Auger electron. In the first case the X-ray final energy will be equal to the energy difference between the two levels involved (E_1 and E_2 with $E_1 > E_2$) and will be independent on the initial photon energy:

$$E_f = E_1 - E_2 \quad (2.2)$$

In the Auger event, instead, this energy will be used to release an electron from another level, leading to three levels involved. Therefore, the Auger electron final energy will be:

$$E_f = (E_K - E_{L_1}) - E_{L_2} \quad (2.3)$$

Where E_K , E_{L_1} and E_{L_2} are energy of the levels K (1s), L_1 (2s) and L_2 (2p) that give the name to the process (KL_1L_2). Note that E_f is independent on the initial photon energy.

However X-ray emission and Auger emission are competitive processes: Auger process is favored against fluorescence for atoms with low atomic number. It is also important to notice that in general the photoelectron is much more energetic with respect the Auger one.

2.3 The Local Effect Model and its limitations

Since the process that induces an irradiated cell to death is fully guided by biological variables, it is difficult to have a fully mathematical description of it. The Local Effect Model (LEM) is the most used to evaluate the effects of a radiation event and the tissue response after photon hitting. Here, the concept of local dose is used, defined as the mean energy deposition in any point of a particle trajectory.

Even if different implementations of the model exist with increasing generalization, the main quantity predicted by LEM is the mean number N of lethal events per cell, induced by the radiation pattern:

$$N = \frac{\ln S_x(d(x, y, z))}{V_{nucleus}} dV_{nucleus} \quad (2.4)$$

where S_x , function of the radiation dose, contains informations of the post-radiation effects, $d(x, y, z)$ is the energy space distribution and $V_{nucleus}$ is the cell nucleus volume.

Harold N. Mc Quaid *et al.*, however, highlight the fact that while the LEM prediction is good for the long term effects on cell DNA, it doesn't simulate the short term ones. In order to develop a more complete model of the process, it is important to define the position of the GNP with respect the nucleus. Depending on the cell type and on the dimension of the particles, they will be at a certain distance from the nucleus. This is an important parameter considering the different mean free paths between Auger and photoelectrons. In fact, while the first ones are able to deposit energy up to a distance of 1.5 μm in water (according to their energy), the photoelectrons, much more energetic, can have a path of 20 μm in water. This leads to the conclusion that while Auger electrons give an effect in the close vicinity of the surface of the GNP, the photoelectrons, having a longer path, will have an higher probability of interaction with a DNA molecule in a cell nucleus. Furthermore, as explained before, the energy of the photoelectrons can be increased, playing with the energy of the incoming X-ray photon.

Let's consider a nucleus with radius R and a GNP releasing an electron (consider the source as a point) as represented in figure 2.1. Since the electron can potentially go in all direction, let's consider a sphere of penetration of radius r . If the sphere of penetration intersects the one representing the nucleus, there will be a certain probability of interaction in which the electron energy (E_D) can be deposited in the nucleus. Assuming an homogeneous distribution of GNP around a cell nucleus, E_D is given by:

$$E_D = \frac{E_e V_i}{4/3\pi r^3} \quad (2.5)$$

where V_i is the intersection volume. Note that $V_i = 0$ when $r < d - R$; this condition describes electrons that don't have enough energy to reach the nucleus. On the other hand, if $r > d + R$ then $V_i = 4/3\pi R^3$, the electrons with high penetration distances and high energies are taking into account. From (2.5), the deposited dose D in the nucleus is proportional to:

$$D \sim \frac{E_D}{\rho V_n} \quad (2.6)$$

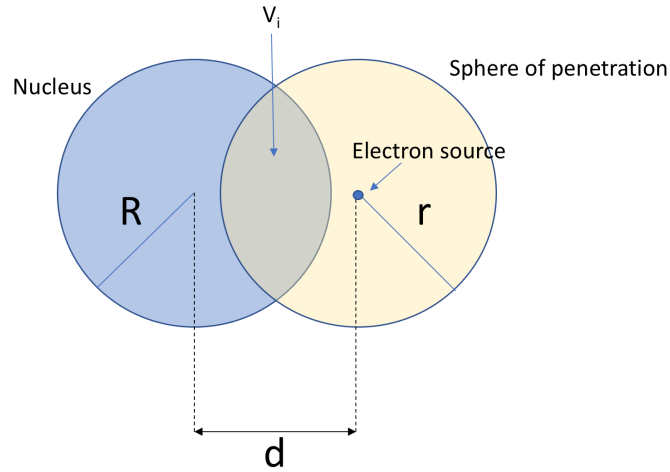


Figure 2.1: Schematic representation of the interaction between the cell nucleus and the sphere of penetration of an electron emitted by a point source

where V_n is the nucleus volume and ρ is its density (wt/vol). Starting from this quantities, it is possible to evaluate the radiation enhancement due to ionization:

$$enh \approx w\mu \frac{E_e}{E_{hv}} \quad (2.7)$$

where w is the ratio between the gold present and the total weight of the considered tissue, μ is the ratio between the mass attenuation energy of gold in the material and in water, E_e is the electron energy and E_{hv} is the photon energy.

In conclusion, the model of Harold N. Mc Quaid *et al.* evaluates the gold radiation enhancement effect on cells and tissue and one of its outcomes is that the long term DNA damage is given mostly by Auger electrons because even if their energy is low, it can be enough to produce lesions able to trigger biological processes leading to cell apoptosis and consequent death. On the other hand the short term damage (about a hour) is driven by photoelectrons that can lead to an immediate effect thanks to their higher energy.

Chapter 3

Materials and methods

3.1 Gold nanoparticles

I synthesized and characterized GNPs of two different sizes: one batch of expected diameter of about 3-4 nm (called from now on small Gold Nanoparticles, sGNP) and another one of expected diameter of about 40-50 nm (called from now on Big Gold Nanoparticles, BGNP). The idea, in fact, was to perform all the experiments using both the diameters and to perform a size dependent study. However, due to a lack of time, this was not possible and in this thesis only the experiments with sGNP are reported. However I chose to report the synthesis and characterization results for both the sGNP and BGNP. For the two batches, two different synthetization techniques have been used. Particles characterization includes the size, the z-potential, the absorbance and the concentration analysis. Briefly, the techniques will be described in the following.

3.1.1 Synthesis

Small Gold Nanoparticles

The particles were synthesized thorough the reduction of chloroauric acid $H[AuCl_4]$ by using the following protocol.

First of all a solution with 1.2 mL 1N NaOH in 120 mL of Milli-Q water is done. In another beaker a solution of 33 mL of MilliQ water with 400 μ L of THPC (tetrakis-(hydroxymethyl)-phosphonium chloride) is made. 4 mL of this solution are added to the NaOH one and let it stir for 5 minutes at a speed of 350 rpm. Finally, 6.75 mL of aged (at least 3 days) 1% chloroauric acid is quickly poured in the stirring beaker (high stirring speed). This last

step is critical: in order to have the particles as monodisperse as possible, there must be just one nucleation center during the reaction. If the acid would be slowly poured, more nucleation centers would be created leading in different diameters among the particles. The resulting particle size immediately after the reaction should be very small (1-2 nm of diameter), but after letting the sample age for at least 2 weeks at -4°C , it aggregates till reaching stability, increasing the dimension till about 4 nm. In order to increase sample concentration, for each particles batch, 10 mL of Au GNPs were put in a uncap 50 mL centrifuge tube and let the water evaporate in a desiccator (a low vacuum chamber) for about 5 days till reaching the 3 mL level. In fact, due to the very low particles dimension, it was not possible to concentrate them with centrifugation.

Big Gold Nanoparticles

In the following, the protocol used for the synthesis of BGNP:

In a beaker combine 100 mL of MilliQ water and 1 g of citric acid with a stir bar to obtain aqueous citrate solution. Let dissolve on stir plate. Separately in an Erlenmeyer flask add 100 mL of MilliQ to 1 g of gold chloride 99.99% and swirl around to dissolve. Filter the aqueous gold chloride solution under vacuum in the hood with a $0.2\ \mu\text{m}$ filter. Cover the filtered flask with aluminum foil. Separately boil 100 mL of MilliQ water. Once boiling add 0.8 mL of aqueous citrate solution and then 1ml of gold chloride. Watch the changing of the color from a dark gray to yellowish and again to red.

To concentrate the sample, thanks to the relatively big diameter of the particles, it was possible to use a centrifugation method.

3.1.2 Characterization

Size

Small particles (sGNP) diameter was evaluated through Atomic Force Microscopy (AFM) and Transmission Electron Microscopy (TEM). Big particles (BGNP) diameter was measured through Dynamic Light Scattering (DLS).

AFM Briefly, the AFM is a microscopy technique that analyzes the sample through a micrometric tip attached to one extremity of a cantilever. The tip can scan the sample with a nanometric resolution thanks to piezoelectric actuators (either the sample or the tip can move according to the microscope). When the tip is in close proximity to the sample, a weak force establishes between the "few" molecules of the tip and the specimen surface, mostly of Van der Waals type. If the force is kept constant during the scan, the tip will

band, following the topography of the surface in order to keep constant its distance from the sample while moving, "drawing" exactly its profile. A laser is exploited to create a feedback signal. The photon beam hits the back part of the cantilever in correspondence of the tip and it reflects on a photodetector, able to detect different reflection angles, from which the exact height of the tip (and consequently of the sample) can be evaluated. The final result is a false color map of the sample surface that indicates the height of each point of the surface. It is easy to understand the importance of having a superflat surface on which the sample is placed. This role is plaid by the *mica*, that can accomplish the need of a surface with a very low roughness.

The sample was placed on the stage, using PGE polymer as stabilizer and the instrument used for this type of characterization was a MultiMode AFM from *Bruker* with tapping technology.

TEM In this technique the sample is bombarded with high energy electrons and they are collected below the stage. This means that we will have black spots in correspondence to the atoms of the sample that don't allow the electrons to pass through, while the other regions will be lighter. The resolution can reach the atomic level and it is possible to see the lattice orientation of the sample. Since the electron beam has to pass through, the specimen was put on an ultra-thin carbon grid in a very low concentration. For this reason, the samples were diluted 100 times and just few micro-liters were put on the grid. The measurements were performed at Rice University (Houston, TX) in the department of mechanical engineering with a TEM-2100F from *JEOL*[®]

Dynamic Light Scattering Dynamic Light Scattering is a widely used technique for measuring the particle size in a suspension thanks to its quickness and to the simplicity of sample preparation.

The measurement involves the scattering of light when it hits a suspension of small particles (Rayleigh scattering). Due to the Brownian motion, the distance between the particles constantly changes giving rise to a fluctuation of the scattering intensity. These fluctuations can be evaluated through the so called second order normalized autocorrelation function [9]:

$$g_2(\tau) = \frac{G_2(\tau)}{\langle I \rangle^2} \quad (3.1)$$

where $\langle I \rangle$ is the average intensity, τ is the correlation time and $G_2(\tau)$ is the temporal correlation function. $g_2(\tau)$ can be related to the first order correlation function:

$$g_1(\tau) = \exp(-q^2 D \tau) \quad (3.2)$$

where q is the magnitude of the scattering vector and D is the translational diffusion coefficient. q can be written as:

$$q = \frac{4\pi n}{\lambda_0} \sin\left(\frac{\theta}{2}\right) \quad (3.3)$$

where n is the refractive index of the solution, λ_0 is the wavelength of the incident light in vacuum, and θ is the scattering angle of light. At the end the (average) hydrodynamic radius of the particles (R_h) can be determined exploiting the Stokes-Einstein equation:

$$D = \frac{kT}{6\pi\eta R_h} \quad (3.4)$$

where D is the diffusion coefficient, k is the Boltzmann's constant, T is the temperature and η is the solvent viscosity.

The measurement was done with a Zetasizer *nano series* from Malvern®. The sample was put in a 4 clear sides plastic cuvette. For the analysis the machine's software was used. Before the measurement few parameters were set: the viscosity, the solvent type and the particle material. It is important to notice that this type of analysis have been done only for the bigger particles due to the low accuracy of that particular instrument. The measurements were, in fact, considered "true" for particles with a diameter greater than 20nm.

Zeta potential

As mentioned above, our GNP sample is a colloidal system, i.e. a suspension of charged particles (phase I) in a liquid phase (phase II). The presence of two phases, leads by necessity, to the formation of a potential difference between the surface of the solid phase and the liquid one.

In particular, if the surface of phase I is negatively charged, positive charges already present in the solution will accumulate in its vicinity forming a charges shell around the particle. In the charged shell, as shown in figure 3.1, there will be a inner layer in close proximity with the solid surface where the ions will be stronger bounded (first layer) and an outer layer in which the ions "feel" in a lower measure the influence of the particle. Here, the electrostatic potential exponentially decreases while going far from the surface of phase I (5-200 nm) [10], into the bulk solution, which potential is consider as the reference one. As a consequence the charges in the second layer are subjected to diffusion.

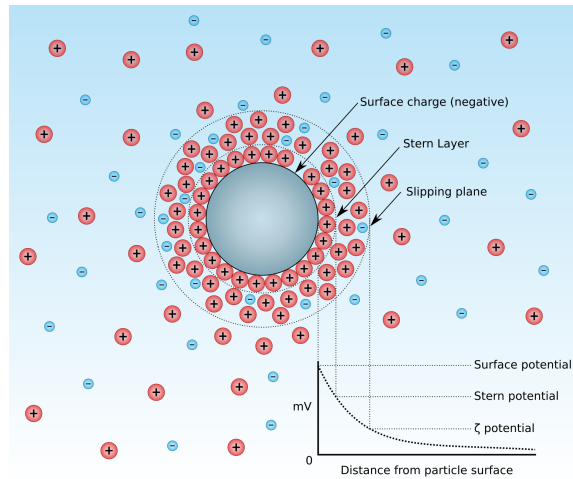


Figure 3.1: Graphical representation of the EDL around a negatively charged particle and zeta potential. Source: Wikipedia <https://it.wikipedia.org/wiki/Potenzialezeta>

This arrangement of charges at the interface is the so called *electrical double layer* (EDL). When one of the phases is forced to move with respect the other (due for example to pressure difference or external electric fields) a set of phenomena can occur called *electrokinetic effects*: electrophoresis, electro-osmosis, streaming potential and sedimentation potential. In all this processes, there is a relative motion between the surface of the particles and the liquid surrounding it. However the so called *surface of shear* can be defined as a virtual surface positioned between the first and the second layer, within which the liquid is considered stationary. This leads to the fact that when the particle is subjected to motion, it will move with its own enveloped liquid layer and charges. The mean potential at the surface of shear is defined as the *zeta potential*.

The zeta potential determines many of the colloidal properties such as adsorption capabilities or interaction energy between particles. This can be correlated to the stability of the particles against coagulation or with the sedimentation behavior of the colloidal itself. The most important quantity that affects the zeta potential is the pH. In fact, considering negatively charged particles in suspension (negative zeta potential), if more alkali is added, the solution will become more basic and the particles will acquire a more negative charge, increasing, in absolute value, the zeta potential. On the contrary, if acids are added, more positive charges will be present neutralizing the particles charge. This condition is the so called *isoelectric point*. Generally speaking, if a colloidal system has a zeta potential $|\zeta| \geq 30$ mV is considered stable.

In the electrophoresis phenomenon, the movement of charges is triggered by an applied electric field across the electrolyte. The particles in the liquid will be attracted by the



Figure 3.2: Special cuvette for Z-potential measurement. Source: Malvern website

electrode of opposite charge. Viscous forces oppose this motion and when equilibrium is reached, the particles will have constant velocity. This is the so called *electrophoresis mobility* (U_E), linked to the zeta potential through the Henry equation:

$$U_E = \frac{2\epsilon\zeta f(ka)}{3\eta} \quad (3.5)$$

where ϵ is the dielectric constant, η is the viscosity and $f(ka)$ is the Henry function, approximated by two possible values: 1.5 (Smoluchowski approximation, for particles greater than 0.2 μm) or 1.0 (Huckel approximation, for smaller particles). Therefore, by measuring the electrophoresis mobility it is possible to evaluate the zeta potential.

The measurement has been done by putting the sample in a 4-clear side plastic cuvette equipped with a special cap with electrodes reported in figure 3.2. After the potential is applied, U_E is measured through the *Laser Doppler Velocimetry* (LDV). In this technique a laser beam hits the cuvette and the scattered light is detected at an angle of 17° . The scattering is combined with the reference beam, producing a fluctuation in the intensity of the scattered light, whose rate is proportional to the speed of the particles.

The instrument used for this type of characterization is a Zetasizer *nano series* from Malvern[®].

Absorbance

The absorbance contributes determine the optical properties of a material. It is important to notice that nanomaterials show different optical properties according to their dimensions. In particular we expect that our samples will have the maximum of absorbance at different wavelengths: a red shift is expected with the increasing of the dimensions.

The light source of the instrument produces a monochromatic photon beam that hits the sample passing through it. Thanks to the detectors, the instrument will measure the ratio between the intensity of the light before (I_0) and after (I) passing through the cuvette, evaluating in this way the transmittance, from which the absorbance can be derived:

$$A = -\log(I/I_0) \quad (3.6)$$

The instrument performs the analysis by scanning among different wavelengths according to the settings. Since from the literature the maximum absorbance of Au colloidal is supposed to be around 550 nm, the wavelength range was set between 200 nm and 800 nm.

The optical analysis was performed with an UV-Vis spectrophotometer located in the laboratory, by putting 500 μ L of sample in a micro-cuvette with two clear sides.

Concentration

For what concern the concentration, two different methods has been exploited: a theoretical prediction followed by a physical measurement performed with an Inductive Coupled Plasma Mass Spectrometer (ICP-MS).

Theoretical prediction Haiss *et al.* derive in their paper [11] an equation suitable for the determination of the concentration of a colloidal starting from the size, the maximum absorbance of the sample and few parameters that they evaluate in their experiment. The proposed equation is the following:

$$d = \left(\frac{A_{spr}(5.89 \times 10^{-6})}{c_{Au} \exp(C_1)} \right)^{1/C_2} \quad (3.7)$$

Where A_{spr} is the plasmon resonance absorbance, d is the diameter of the particles (nm) and c_{Au} is the concentration of the sample (mol/L). C_1 and C_2 are constants that can be evaluated experimentally. In fact, plotting the linear behavior of the extinction coefficient at the surface plasmon resonance by varying the particles diameter, C_1 can be defined as the intercept and C_2 as the slope of the line. Since it was not possible to vary the diameter of the particles, the two constants were taken from [11], choosing the theoretical ones: $C_1 = -4.70$ and $C_2 = 0.3$. The only unknown is c_{Au} assuming the diameter found with AFM.

ICP-MS measurement The ICP-MS analysis was performed at "Rice University" (Houston, TX) in the department of *Bioscience Research*. I was trained to use the instrument and to prepare the specimen.

For the measurement, the sample has to be completely dissolved. For this reason aqua regia (3 : 1HCl : HNO₃) was synthesized and used to dissolve gold NPs. This was further diluted in 2% HCl till reaching a certain concentration evaluated starting from 3.7). Then, a calibration curve has been done with 5 points around the hypothetical concentration of the sample. So a gold standard was bought with a known nominal concentration of 1000 µg/mL 5 dilutions of the standard were made and measured by the instrument for the calibration: 10 µg/L, 50 µg/L, 500 µg/L, 5000 µg/L and 10000 µg/L. After the calibration, the measurement of the sample can be run.

As mentioned in chapter 1.3, even though GNP of both sizes will be analyzed from the characterization point of view, only the smaller ones will be employed in the experiments.

3.2 Lewis Lung Cells

The Lewis carcinoma is a mouse lung tumor studied by Dr. Margaret R. Lewis in 1951. Some of the primary cells had been isolated and a new cell line started (LLC1). Being highly tumorigenic for C57B1 mice, they are often used to induce tumors for anti-tumoral treatments studies.

The first passage of cells were purchased from the company *American Type Culture Collection* (ATCC®- CRL-1642™). According to the literature [12], they were cultured by using the Dulbecco's Modified Eagle Medium (DMEM) in flasks of 75 mm² surface (called T75) and periodically split when reaching a confluency ¹ of 85%-90%. LLC appear rounded, slightly attached to the surface and have a population doubling time of about 21 hours. They tend to grow as a single layer on the plastic surface and if the coverage reaches 100% they start to place one over the other creating a non-healthy environment that brings the cells to death. Optical images are reported in figure 3.3. The cells were grown in an incubator with a controlled atmosphere: 37 °C and 5% CO₂.

3.2.1 Cells splitting, counting and cryo-conservation

In the following it is briefly reported the protocol followed for the splitting of the cells and for their conservation. Each splitting is consider a new generation of cells, so they pass from passage x to passage $(x + 1)$

¹The confluency is a measurement of the cells coverage percentage of the flask surface.

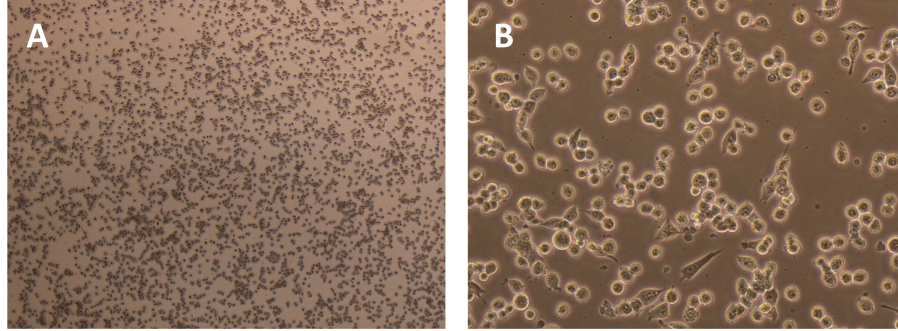


Figure 3.3: Images of Lewis Lung Cells passage 1 from optical microscope. (A): 4x magnification; (B): 20x magnification

The splitting has to be performed whenever the cell confluency reaches 85%-90%. All the process must be followed in the hood to avoid contamination. The operator has to wear gloves and lab coat. Before starting, the hood and the gloves have to be sprayed with ethanol for bacteria disinfection.

1. With the help of an aspirator connected to the vacuum line in the hood, remove all the media in the flask
2. Wash the flask to ensure completely remotion of the media with 10 mL of 1X Phosphate Buffered Saline (PBS) and remove it with the vacuum line after having gently shake the flask
3. Add 2 mL of 1X Trypsin-EDTA (Ethylenediaminetetraacetic acid) 0.25% and incubate for 5 min. The trypsin dissociates the bindings cell-cell and cell-flask, detaching completely the cells. Note that the trypsin is quite toxic for the cells so the timing is very important. To help the process, the flask can be gently shaken.
4. With a sirological pipet collect the cells from the flask and merge them in a 50 mL centrifuge tube, adding DMEM media in a volume at least equal to the one of the trypsin
5. After mixing, take 10 μ L of cells and put them in a 0.5 mL eppendorf centrifuge tube with 10 μ L of trypan blue, a die able to stain the cells.
6. After mixing collect the 20 μ L and put it on the proper slide for cells counting.
7. The counting has been performed with the *Cellometer*[®] from *Nexcelom Bioscience*. The instrument gives the number of living cells per milliliter. One can evaluate the number of cells in the entire volume contained in the 50 mL centrifuge tube and take the right amount for next generation cell colturing. For a T75 flask the amount

is 8.25×10^5 cells per flask.

8. Centrifuge the remaining cells at 200 G for 10 min.
9. Discard the supernatant and mix the cell pellet with a freezing media composed by 95% Fetal Bovine Serum (FBS) and 5% Dimethyl sulfoxide (DMSO). The DMSO will stabilize the cells especially in the future thawing phase
10. Put the cells in cryotubes and put them at -80 °C for conservation. In order to avoid thermal shock, put the cryotubes in a plastic box containing isopropanol alcohol (IPA) that allows a decreasing of the temperature with a rate of 1 °C/min.

3.2.2 LLC Luciferase gene expressing

Lewis Lung cells have been engineered in order to express the firefly luciferase gene for subsequent *in vivo* bioluminescence imaging. The expression is an important tool not only for the detection of the labeled cells and cancer progression *in vivo*, but also for the verification of proliferation of a certain cell line *in vitro* [13] [14].

In particular, the third passage of LLC was thawed for processing the gene expression. Dr. Pathak's lab took care of the engineerization. In order to stabilize the new cell line, several splitting steps have been performed before *in vivo* experiments. Furthermore they have been cultured in the usual media with the adding of 1% of Geneticin, an antibiotic selective for the non luciferase expressing cells. In this way the expression is guaranteed also in future cell generations. Due to this selective elimination of cells, the doubling time slightly increased.

3.3 CAM model

Here the protocols for the "operations" involving the eggs will be described. Before that, few general details will be clarified. After their delivery to the lab, they were stored in a special portable incubator containing a maximum of 50 eggs at a temperature of 37 °C with an underneath water bath to ensure constant humidity and allow good chicken embryo growth. At the end of each experiment they have been sacrificed by hypothermia by putting them at -20 °C.

3.3.1 Opening the egg

In order to allow the inoculation of cells on the membrane, firstly the egg has to be opened and a little window created in the upper part of the shell. For this reason a little hole is

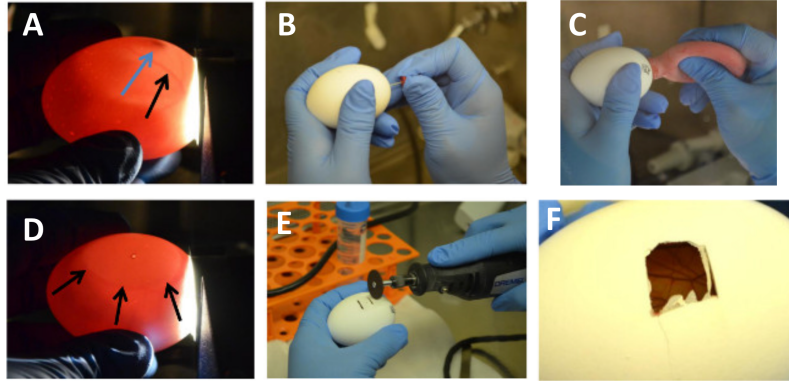


Figure 3.4: Images from [5]: (A): Identification of embryo (blue arrow) and vessel (black arrow) using the candler. (B): The hole is made with the needle. (C): Creation of the air sac. (D): Verification of the successful dropping of the CAM away from the shell. (E)-(F): Opening the window with the little saw and final result

opened with a needle between the two major vessels of the egg (they can be seen by illuminating the egg through the shell with an egg candler). Now, air is pumped inside with a little rubber bulb in order to gently detach the membrane from the inner shell and to create an air sac underneath. After this, a little saw can be used to create a window of 1 cm x 1 cm. Then a silicone ring of 1 cm of diameter is put above the membrane. This will ensure a localization of the cells when inoculated. Then a scotch tape is put on the window to protect the egg. To have a clearer idea of this process, look at figure 3.4.

3.3.2 Inoculation of cells and tumor growth

To inoculate the cells, the protocol described in Dr. Pathak's paper was used [5]. In particular, for each *in ovo* experiment, the cells were given to Dr. Pathak's lab after the splitting. After counting them, the cells were transferred in 50 mL centrifuge tubes in ice with 1 million cells per tube in normal media after centrifugation. Subsequently, they were suspended in a solution of 60% matrigel² and 40% PBS for the inoculation on the CAM, taking into account that the maximum volume that the silicone ring can hold is 100 μ L and that the number of cells per egg can range from 500000 to 2 million according to the cell line [5]. After that, the desired amount of cells were pipetted in the center of the silicone ring. Note that the matrigel polymerizes at room temperature and its high viscosity ensure a more accurate localization of the cells in the silicone ring.

After three days of incubation tumors were well visible on the CAM, as can be seen in

²Matrigel: gelatinous polymer, solid at room temperature



Figure 3.5: Examples of LLC derived tumors on CAM after 3 days of incubation. It is clear (especially in (B)) the presence of the carcinoma and its 3D shape.

an example in figure 3.5. It is important to say that the ideal shape of the tumor is a 3D nodule, but it can happen that a sheet-like tumor develops along the surface in the silicone ring with a certain thickness. The final shape depends on the way of the inoculation of the cells and their health, but also on the vascularization of the tumor. In other words, the shape and dimension of the tumor is egg dependent and can not be predicted.

3.3.3 Gold nanoparticles on CAM

Taking into account that there were nearly no references for the inoculation of gold nanoparticles on CAM, a couple of methods have been tried. At the end, the best resulted to be the inoculation of the gold nanoparticles right at the same time of the cells inoculation. In particular the desired amount of particles were suspended in the solution with the cells, the matrigel and the PBS and than inoculated all together, without changing the PBS/matrigel ratio.

The other technique we tried was to inject the particles with a needle in the tumor after its formation (intratumoral injection), but this solution immediately presented some problems. First of all, the injection had to be done manually and there was not the perception of the needle inside the tumor, so there was the risk to inject the particles underneath. Secondly the injection implies a localization of the particles in one point, eventually preventing the radioenhancement effect to the whole tumor. On the contrary, the inoculation of the particles with the cells allowed a uniform distribution, since the tumor would embed the particles while growing. A particular pathological staining was used to being able to visualize the particles embedded in tumor tissue: the silver stain. More details in chapter 4.2.2.

3.3.4 Tumor harvesting and histology

When the tumor has to be collected, as shown in figure 3.5, is well visible on the CAM. In order to collect it, first of all the egg is put for 30 minutes at -20 °C in order to sacrifice

the embryo. Then the window already opened in the shell is enlarged by using a pairs of pliers. The silicone ring can be removed and gently the tumor can be slightly pulled up. The CAM is cut all around the tumor. This is a critical step because the operator has to pay attention and to take as much tumor tissue as possible leaving the CAM in the egg for a good pathological result. Then the tumor is put in PBS for washing away any blood residue. Subsequently the tissue is fixed in 10% paraffin.

The paraffin blocks were always sent to the pathology core of the Houston Methodist Research Institute for histology (slicing and staining).

The tissue staining is a way to mark different parts of the sample in order to visualize it under the microscope. One of the most used stain for histology is the so called H&E whose acronym stands for Haematoxilin and Eosin. It allows to visualize and distinguish among different components in a tissue. The final tissue colors vary from blue, violet and red. In particular haematoxilin is a positive and basic compound that easily binds to DNA and RNA (acidic and negatively charged), staining with a dark blue the cell nucleus. On the other hand the eosin is acidic and negatively charged and it binds easily with some positive proteins present in the cytoplasm, staining it with a red or pink colour. An example is reported in figure 3.6 where a LLC tumor derived in CAM is represented. It is important to distinguish between the tumor (mouse cells) and the chicken cells all around. However this can be easily done noticing that the nuclei of tumor cells are way bigger than the chicken ones. It is interesting to notice the presence of vessels inside the tumor mass that have been perpendicularly cut. The red blood cells are well visible and characterized by nuclei. This is a peculiarity of wingeds.

3.4 Radiation equipment

For radiation experiments, a biological X-ray irradiator was used: the RS-2000 from *RAD SOURCE* with the concession of Dr. Pandey's research group from the department of Radiation Oncology of the Houston Methodist Research Institute. The machine, reported in figure 3.7, has an X-ray tube without a radioactive source, so it is quite safe. Furthermore, in the chamber some concentric circumferences are drawn. They correspond to the exposed fields. The operator has to place the body to irradiate inside one of this circles according to the radiation level that one wants to achieve. A summary table is represented in figure 3.8. So, for example, if I want to irradiate an object with 2 Gy, I have to preselect the level (that in this case correspond to Level-0), and put the object inside the corresponding circle (in this case the greatest). Finally the operator has to set the time required to reach the desired dose (in the example about 30 s).

The same machine was used both for eggs and mice irradiation. Since the dose delivered to the eggs was always quite low, 6 eggs at a time were irradiated thanks to the high irradiation field. On the other hand, because of the high dose for the mice (up to 20 Gy), it was

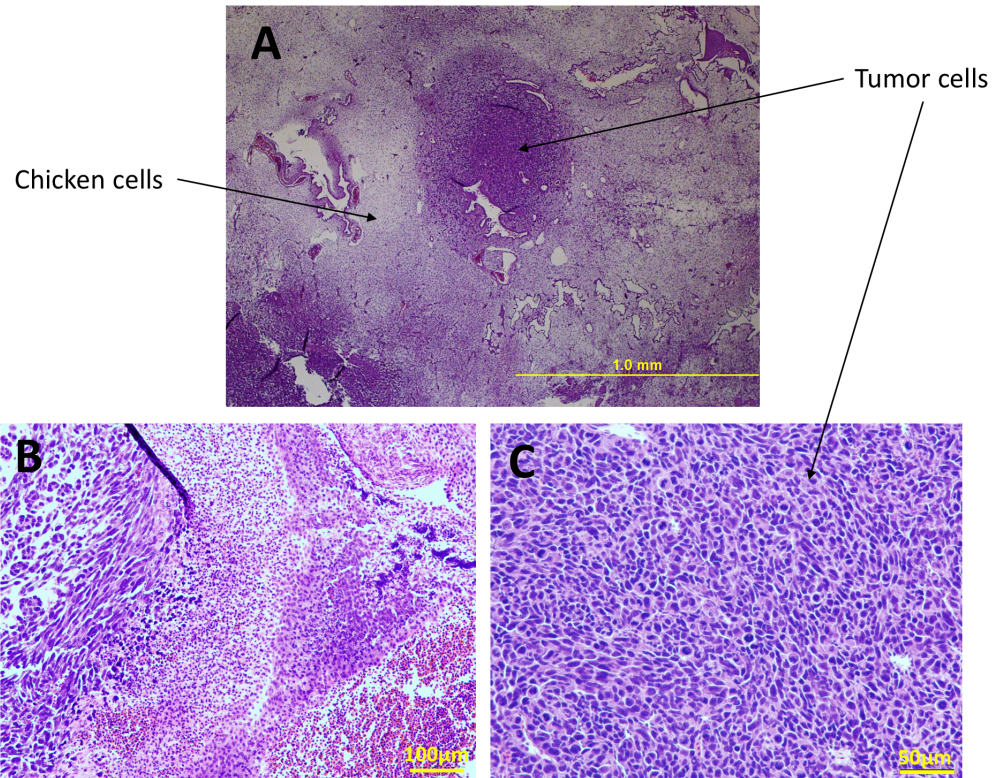


Figure 3.6: Images of LLC tumor derived in CAM acquired with optical microscope *Olympus BX-UCB*. (A): 4x magnification; (B): 10x magnification; (C): 20x magnification.

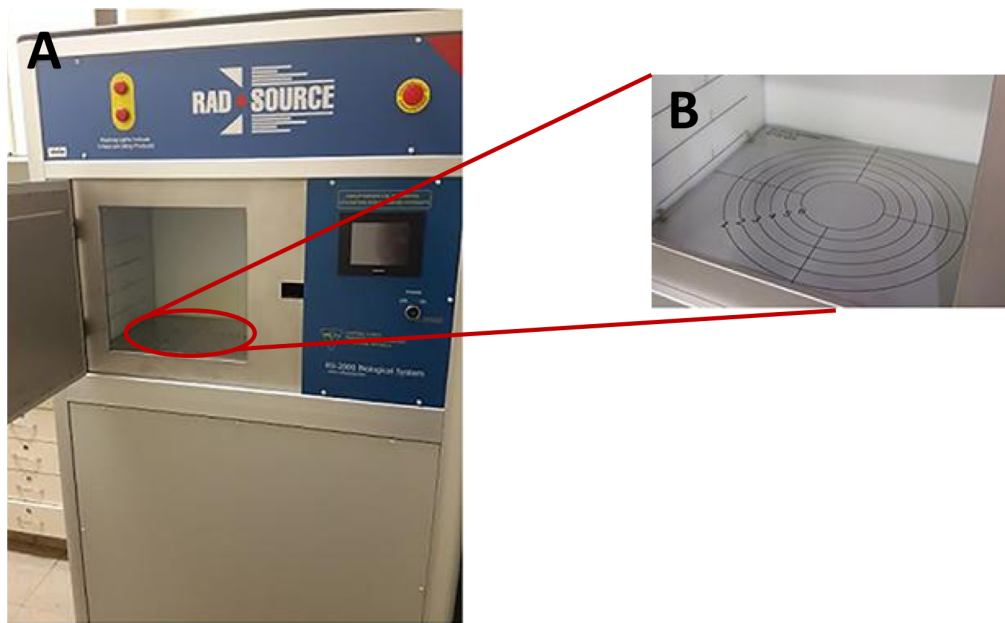


Figure 3.7: (A) Radiation equipment used for experiments, general view. (B): magnification of the internal part of the chamber. Note the circumferences that define the different zones for different doses.

Source: http://www.scielo.br/scielo.php?pid=S0100-879X2017000300607&script=sci_arttext

Levels	Output (Gy/min)	Source distance (mm)	Field diameter (mm)
Level 7	59.0	118	75
Level 6	24.3	184	118
Level 5	13.5	247	63
Level 4	8.7	308	206
Level 3	5.9	373	250
Level 2	4.3	437	294
Level 1	3.3	501	337
Level 0	2.9	530	357

Figure 3.8: Table of the levels and corresponding outputs in Gy/min.

Source: <http://www.radsources.com/rs-2000-pdf-brochures/>

possible to irradiate just 2 mice at a time due to the smaller circumference. Furthermore, when mice were present a lead shield was used to protect the vital parts of the animals (head and body) and to irradiate the tumor only.

3.5 Bioluminescence and IVIS imaging

As explained before, the use of luciferase gene expressing cells allows to visualize the tumor progression with simple imaging tools in a non invasive manner. This exploits and mimics the bioluminescence phenomena that happens also in nature in different organisms: fungi, bacteria, but also fishes and insects. In his paper, Hastings J.W. presents a review of the principal bioluminescence reactions [15], explaining the main mechanism that, in general, involves the presence of luciferase proteins called also Lase:

“Biochemically, all known Lase are oxygenases that utilize molecular oxygen to oxidize a substrate (a luciferin; literally the "light-bearing" molecule), with formation of a product molecule in an electronically excited state”.

So, the presence of the substrate is essential and, in our case, it is injected right before the imaging. Furthermore, to activate the reaction, the luminescent body is excited with a light source, and the emitted light is collected by a CCD camera that allows the reconstruction of the image. The instrument used for this purpose is called In Vivo Imaging System (IVIS[®]) and was used for both eggs and mice. An example of image is reported in figure 3.9. We chose to image one egg at a time due to image saturation reasons, while, thanks to the anesthesia machine connected to 5 nose cones inside the machine, we were able to image 5 mice at a time. Note that the software superimposes the optical image (in gray scale) taken by a normal camera and the luminescence signal, represented by a color scale. The unit of measurement is [counts/sec] so that images with different exposure times can be compared. However as can be noticed in figure 3.9, the mice image has a different unit of measurement. That's because we collected all the mice images several time after the egg experiments and we acquired experience and confidentiality in using the machine and we realized that the *radiance* unit is the most used in literature. This doesn't imply a less significance in the eggs experiments results. The images obtained with this tool give informations on the dimension of the tumor mass and the intensity of the signal detected. Furthermore, in the image post-processing, it is possible to quantify the Region Of Interest (ROI) useful for the data and outcomes evaluation.

The IVIS used for our experiments was from *Perkin Elmer*[®] (see figure 3.10), located in the animal facility of the Houston Methodist Research Institute.

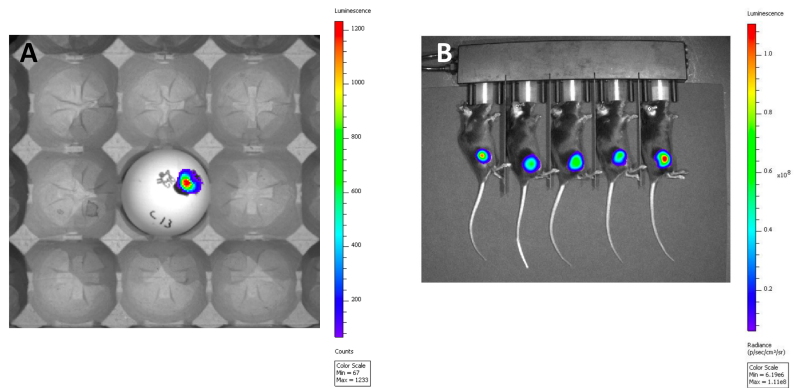


Figure 3.9: Examples of IVIS images. (A): egg image; (B) mice image.



Figure 3.10: Picture of IVIS and schematic of its more important components.
Source: <http://www.perkinelmer.com>

Chapter 4

Experiments design

In the following the design of the done experiments will be presented dividing them in: *in vitro*, *in ovo* and *in vivo* experiments. Once again, remember that only the smaller nanoparticles will be used in all the experiments.

4.1 *In vitro* experiments

4.1.1 Evaluation of growth rate of Lewis Lung Cells luciferase expressing

Since the engineerization of LLC in LLC-Luc brought an increasing of the cells doubling time, as reported in chapter 3.2.2, this experiments want to evaluate if the cells are still suitable for *in ovo* and *in vivo* experiments. In other word we wanted to see if the luciferase expression persists also in the progeny of the engineered ones, evaluating the growing curve of the LLC-Luc. This was done exploiting the bioluminescence of the cells and IVIS imaging.

The LLC-Luc were cultured in a 96 walls plate with different starting numbers of cells:

Group 1: 100000 cells in 3 walls

Group 2: 50000 cells in 3 walls

Group 3: 25000 cells in 3 walls

Group 4: 12500 cells in 3 walls

Group 5: 6250 cells in 3 walls

IVIS images were acquired during the next 4 days in order to monitor the signal. In this case the ROI was used as significant parameter and, of course, an increasing trend is expected.

4.1.2 Cellular uptake *in vitro* study

The objective of this simple experiment is to verify if the particles are successfully internalized by the cells or if they set outside the cell membrane. This was done through TEM microscopy. The sample preparation is critical and it was performed by the imaging team of the Houston Methodist Research Institute.

Several are the methods to prepare biological specimens for TEM imaging [16], but briefly the principal steps are the following:

1. Trypsinization and collection of the cells
2. Centrifugation and washing
3. Fixation with a proper fixant
4. Dehydration
5. Embedding
6. Sectioning of the obtained blocks

100 μ L of GNP were put in the media of LLC in a T75 flask and incubated for 24 hours. Then they were trypsinized and collected in a tube and gave to the imaging lab for sample preparation.

4.1.3 *In vitro* radiation experiments

The first objective is to demonstrate the action of particles plus radiation in a colony of Lewis Lung cells, so at the cells level (*in vitro*) and to demonstrate the low toxicity of gold. For this purpose, two assays were performed with the help of Dr. Arvind Pandey: the comet assay and the clonogenic assay. The aim is to see the different responses of the cells to radiation alone and to radiation plus nanoparticles. Let's enter for a moment into the details of the two assays.

Comet assay: working principle

The comet assay allows for the detection of DNA damage brought, in this case, by the X-ray radiation action that should be enhanced when gold nanoparticles are present.

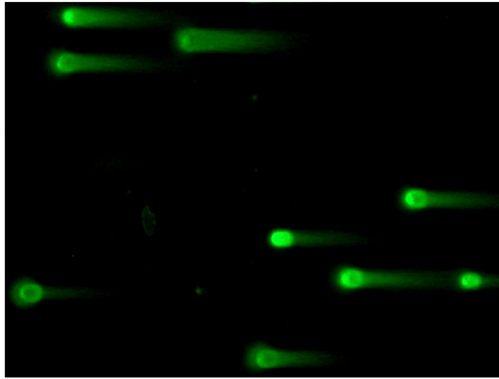


Figure 4.1: Image representing a result example of comet assay. Note the characteristic comet tail that represents the migration of DNA fragments in presence of an applied electric field (electrophoresis) after DNA damage. Each "comet" is a cell.

When damaged, single strand and double strand DNA break in fragments that can migrate in the presence of an electric field (electrophoresis) [17]. This is the principal phenomena exploited in comet assay, even if in the years it has more and more improved, for example with the adding of alkaline components to increase selectivity and reproducibility.

Briefly, very few cells are collected and immobilized in a special slide with a lysis buffer solution. Then the electrophoresis and the stain is performed. The stain allows for a labeling of the DNA fragments that can be then visualized. An example is reported in figure 4.1. Each "comet" is a cell and the circular part represents the nucleus with NOT broken DNA, while the migrated fragments constitute the characteristic "tail" giving rise to the comet shape. By measuring the intensity of the tail (linked to the percentage of damaged DNA) and its length (the so called tail moment) from the image, it is possible to quantify the DNA damage.

Clonogenic assay:working principle

The clonogenic assay was introduced by Puck and Marcus in 1956 with the purpose of checking the survival rate of cells after radiation chemiotherapeutic treatment [18]. It is important to introduce the concept underlined by Munshi *et al.* [19]:

“[...] a cell that retains its ability to synthesize proteins and DNA and go through one or two mitoses, but is unable to divide and produce a large number of progeny is considered dead. [...] a cell that is not reproductively dead and has retained the capacity to divide and proliferate indefinitely can produce a large clone or a large colony of cells

and is then referred to as "clonogenic"

Summarizing, this assay is useful to verify the interruption of clonogenic activity of cells colonies due to, in our case, radiation therapy, monitoring the reproduction rate of the cells in a Petri dish. The results will be given in form of percentage of the plate area covered by the cells. Of course a lower percentage for treated cells is expected.

Experiment design

Passage 4 of LLC was used, coltured in T25 flasks (surface of 25 mm²), since just very few cells were needed. The cells were treated with 50 µL (about 27 µg of gold) of small gold nanoparticles (about 3.5 nm of diameter) dispersed in the media and incubated for 24 hours. Than the cells were irradiated with two different doses: 2 Gy for the comet assay and 3 Gy for the clonogenic one. Summarizing, the groups for this experiment were:

Comet assay:

Group 1: Untreated (Control)

Group 2: Treated with X-ray (2 Gy)

Group 3: Treated with sGNP (50 µL)

Group 4: Treated with X-ray (2 Gy) + sGNP (50 µL)

Clonogenic assay:

Group 1: Untreated (Control)

Group 2: Treated with X-ray (3 Gy)

Group 3: Treated with sGNP (50 µL)

Group 4: Treated with X-ray (3 Gy) + sGNP (50 µL)

4.2 *In ovo* experiments

Since, to the best of our knowledge, this was the first time that murine LLC were inoculate on CAM, few preliminary experiments were performed in order to stabilize an effective protocol for this cell line. In fact, the final vascularization level, shape and dimension of

the tumor can be cell line dependent.

4.2.1 Preliminary experiment: optimization of the initial number of cell

It is important to notice that the number of initial cells inoculated on CAM is not directly proportional to the final dimension of the tumor. According to their distribution, the cells can form a nice nodule (especially if they are near vessels) or can form just a small nodule that falls into a sheet. There is no way to predict the final tumor shape. Furthermore above a certain threshold of initial cell number, the cells start to send apoptosis signals that bring them to death, giving rise to a non satisfying final result. On the other hand, thanks to previous experiments and to the wide experience of Dr. Pathak, it can be said that, once find the optimal cell number, we can expect mainly the same type of growth for future experiments.

Dr. Pathak suggested to start with three different numbers of initial cells: 500000, 1 million and 2 million. Passage 5 of Lewis Lung cells was used and three groups were designed with three eggs each for statistical reasons:

Group 1: 500k cells in 3 eggs

Group 2: 1M cells in 3 eggs

Group 3: 2M cells in 3 eggs

The eggs were then incubated for three days and then the tumors were harvested and fixed in paraffin for histology.

4.2.2 Preliminary experiment: optimization of the amount of gold in the eggs

The objective of this preliminary experiment is the optimization of the insertion of GNP on the CAM and its maximum quantity borne by the egg without being toxic for the chicken embryo. As outlined in chapter 3.3.3, we tried unsuccessfully to inject the particles intratumorally with a needle, but the fragility of the system made this impossible. So the best method resulted to be the inoculation of GNP on the CAM together with the cells, ensuring in this way an uniform distribution in the tumor that would surround the particles.

For testing the maximum amount of gold borne by the egg, three experimental groups were designed with three different volumes:

Group 1: 25 μ L sGNP in 3 eggs

Group 2: 50 μ L sGNP in 3 eggs

Group 3: 100 μ L sGNP in 3 eggs

The starting number of cells was the optimal one found in the last experiment: 1 million cells from passage 8. The eggs were then incubated for three days and then the tumors were harvested and fixed in paraffin for histology.

We tried also to visualize the particles in the histological sample with simple optical microscopy. Due to the low dimension of the GNP this was possible only with a special type of stain: the silver stain. This particular tool allows for a deposition of silver on the gold nanoparticles present in the tissue, increasing their diameter up to the range of micrometer. We were able to visualize them with dark field optical microscopy with oil objective and a magnification of 100x.

4.2.3 Preliminary experiment: optimization of X-ray dose for eggs

The objective of this experiment is to evaluate the maximum radiation dose that the egg can bear and set the right amount of X-rays in order to have just a partial damage to the tumor, still being able to see clearly the further enhancement effect of GNP in future experiments.

Dr. Pathak suggested for this experiment to increase slightly the amount of inoculated cells to 1.5 million per egg since the radiation may shrink the tumor dimension. The passage of the cells was the 14th.

For what concern the dose, we decided to try both a single radiation dose and a fractionated one, usually preferred in clinical treatments. In fact, the first session of radiation hits the metabolic active cells that partially die. In the recovery time, the tumor recruits the so called quiescent cells that, in this way, become active and can be killed with the next radiation session. We tried the 2 Gy and the 4 Gy dose in this combinations:

One dose:

Group 1: Untreated (4 eggs)

Group 2: 2 Gy (6 eggs)

Group 3: 4 Gy (6 eggs)

Two fractionated doses:

Group 4: Untreated (4 eggs)

Group 5: 2 Gy twice at a distance of 48h (6 eggs)

Group 6: 4 Gy twice at a distance of 48h (6 eggs)

Table 4.1: Radiation experiment timeline

	Day 1	Day 2	Day 3	Day 4
Group 1	-	Harvested		
Group 2	2 Gy	Harvested		
Group 3	4 Gy	Harvested		
Group 4	-	-	-	Harvested
Group 5	2 Gy	-	2 Gy	Harvested
Group 6	4 Gy	-	4 Gy	Harvested

Note that both the one dose and the fractionated one experiments have their own control group. This because groups 1, 2 and 3 were harvested the day after the radiation, while groups 4, 5 and 6 the day after the second radiation. The table 4.1 summarizes the experiment and better explains the radiation timeline. Note that *Day 1* is the first day of radiation that was after 3 days from cells inoculation. When harvested, the tumor tissue was fixed for histology (H&E).

4.2.4 Synergistic effect of gold nanoparticles and radiation

After having collected all the preliminary data, we are ready to start the final *in ovo* experiment with the objective to show the radioenhancement effect of GNP. In a first experiment (here not reported) we tried to evaluate the outcomes just looking at the histological slides, but it was impossible to see by eye an effect, since the evaluation of histological sample is too subjective. So we tried to use the bioluminescence and the IVIS imaging. Since the more the intensity of the collected signal, the more the living tumor cells, the idea was to monitor the intensity of the signal over time during the radiation treatment period, expecting a decreasing of the signal after radiation, and a further decreasing when GNP are present. Of course, for this purpose, the LLC-Luc were exploited.

The objective was to have at least 6 eggs per group able to represent the expected results. The eggs were inoculated with 1.5 million of LLC-Luc and irradiated with the optimal fractionated dose 2 Gy + 2 Gy and 4 imaging sessions were performed with the timetable reported in figure 4.2 always doing the imaging before the radiation when happening in the same day.

The groups were the following:

Group 1: Untreated; (6 eggs)

Group 2: Radiation alone (2 Gy + 2 Gy); (6 eggs)

Group 3: GNP + radiation (2 Gy + 2 Gy); (6 eggs)

Day 1		Day 2	Day 3		Day 4
Imaging	Radiation	Imaging	Imaging	Radiation	Imaging



Figure 4.2: Radiation and imaging timeline for the radioenhancement experiment with the eggs

The eggs of group 3 were inoculated with GNP together with the cells (as from the protocol) for an amount of gold of about 15 μg per egg (in a volume of 50 μL)

For the imaging the luciferin was prepared with a concentration of 15 mg/mL and inoculated on the tumor surface exactly 10 minutes before the image acquisition. The action of luciferin, in fact, is time dependent so it is preferable to acquire the image always after the same amount of time to allow the comparison between the different eggs. The volume of luciferin was 100 μL per egg.

4.3 *In vivo* experiments

All the *in vivo* experiments were performed in the full compliance of the ethical principles and upon approval of the protocols by the Institutional Animal Care and Use Committee (IACUC).

In all the following experiments black mice C57BL/6 were used and tumors were induced by injecting subcutaneously in the mouse's flank 1 million of Lewis Lung cells dispersed in PBS .

4.3.1 Preliminary experiment: optimization of radiation dose

Since it is difficult to find in literature a unique protocol for mice irradiation, a preliminary experiment was performed for the optimization of the dose, but also for an establishment of the procedure to follow. We were the first group in the Houston Methodist Research Institute to irradiate mice, so the veterinary team of the HMRI had to create a new protocol with some guide lines to follow. This first experiment was also intended for us to practice with the mice handling in this complex operation. In fact the radiation machine (RAD 2000 from *RAD SOURCE*) was located in the Dr. Pandey's lab in the department of Radiation Oncology of the HMRI and each time the mice had to be transfer from the animal facility to the radiation lab.

Furthermore, the mice had to be anesthetized during the radiation session that, due to the high radiation dose, lasted up to 4-5 min. On the contrary of the IVIS equipment, it

was not present any anesthesia machine inside the radiation chamber, used to maintain the mice narcotized during the radiation time. For this reason in addition to the classical anesthesia, the mice had to be injected with a narcotizing drug right before the irradiation in order to prolong the sleeping time and not to wake up in the irradiation chamber. After having removed the mice from the chamber they had to be injected with an exciting drug to induce the awakening.

For this first experiment 10 mice were used and injected with LLC. The tumors appear superficial in the flank allowing the opportunity to monitor and measure them with a caliper. This type of measurement is very subjective and operator dependent, for this reason it is preferable that always the same person takes the measurements. However, this kind of tumor evaluation is widely used in research and consists in taking two measurements along the longer and shorter axis of the tumor and then for the evaluation of the volume (V_t) this simple operation is applied:

$$V_t = \frac{L \times S^2}{2} \quad (4.1)$$

where S is the shorter axis and L is the longer one.

After 10 days, the mean tumor volume was of about 200 mm^3 and the mice were ready to be irradiated. At this point the mice were sorted in the following experimental groups:

Group 1: Untreated (3 mice)

Group 2: 20 Gy once (3 mice)

Group 3: 14 Gy three times at a distance of 48h (4 mice)

***Ex vivo* experiment for quantification of gold in tumors**

With this experiment we wanted to verify and quantify the amount of gold present in tumors after intratumoral injection by using the ICP-MS. For this reason, $100 \mu\text{L}$ of GNP were injected intratumorally in three mice right before their euthanasia. The tumors were collected and frozen immediately with liquid nitrogen for *ex vivo* processing. In order to make the sample suitable for ICP-MS analysis, the tumors were separately dissolved at high temperature in aqua regia, a solution composed by one part of nitric acid and three parts of chloridric acid, able to dissolve both the organic part and the gold present in the tumors. The obtained solution was then filtered and diluted with chloridric acid. Then the complex protocol explained in chapter 3.1.2 was followed in order to be able to run the measurement. The measurement was run also for a tumor without GNP in order to establish a control. The results will be not reported because a concentration of gold (in

[ppm]) different from zero was found in the tumor without GNP. This can be due to possible residues of gold in the stir bars used for the dissolution of samples and, in general, to a not enough clean procedure followed during the process of sample preparation.

4.3.2 *In vivo* GNP radioenhancement

For this experiment 40 mice were injected with 1 million LLC-Luc. When tumors reached the volume of about 200 mm³ the mice were sorted in groups. Since the radiation amount of the preliminary experiment was too high we decided to lower the dose and, in order to be consistent with the eggs experiment, to triplicate the radiation dose of the eggs, doing an experimental group with 6 Gy repeated two times at a distance of 48 hours. A group with 12 Gy was also designed for a total of 5 groups as follow:

Group 1: Untreated (8 mice)

Group 2: Radiation only (12 Gy) (8 mice)

Group 3: Radiation only (6 Gy x2) (8 mice)

Group 4: GNP + radiation (12 Gy) (8 mice)

Group 5: GNP + radiation (6 Gy x2) (8 mice)

We triplicated also the amount of gold with respect the eggs, so the mice were injected intratumorally with about 45 µg of gold right before each radiation session.

For the IVIS imaging the mice were anesthetized and injected intraperitoneally with 100 µL of filtered and sterile luciferin at a concentration of 15 mg/mL exactly 10 minutes before image acquisition. It was possible to image 5 mice at a time.

Chapter 5

Results and discussion

5.1 Nanoparticles characterization: results and images

The results from the characterization of the two sized nanoparticles are summarized in the table of figure 5.1. As expected, there is a red shift of the absorbance wavelength of the bigger particles. Note that the dimensions from TEM have been extracted from the analysis of the acquired images through the software *ImageJ*, taking in consideration a statistically relevant number of particles. The negative z-potential suggests that the colloids are quite stable. Note that in the table the concentration values are not reported. This because each batch had its own concentration due to the fact that the solutions were put in a desiccator in order to concentrate the GNP (from a volume of 10 mL to 3 mL). In this way the samples had always slightly different concentrations. In figure 5.2, the TEM images of the two type of nanoparticles are reported. Note the beautiful resolution of the instrument that allows to see the crystal orientation of the particles. In figure 5.3 the AFM image is reported: on the right the sample profile from which the diameter was evaluated.

	Diameter (AFM) (nm)	Diameter (TEM) (nm)	Diameter (DLS) (nm)	z-potential (mV)	Absorbance wavelength (nm)
sGNP	3.5 ± 1.5	4.5 ± 1.0	\	-35	522.94 ± 1.42
BGNP	\	33.9 ± 5.5	35 ± 5	-(36.1 ± 2.53)	530 ± 2

Figure 5.1: Summary of the characterization of GNP.

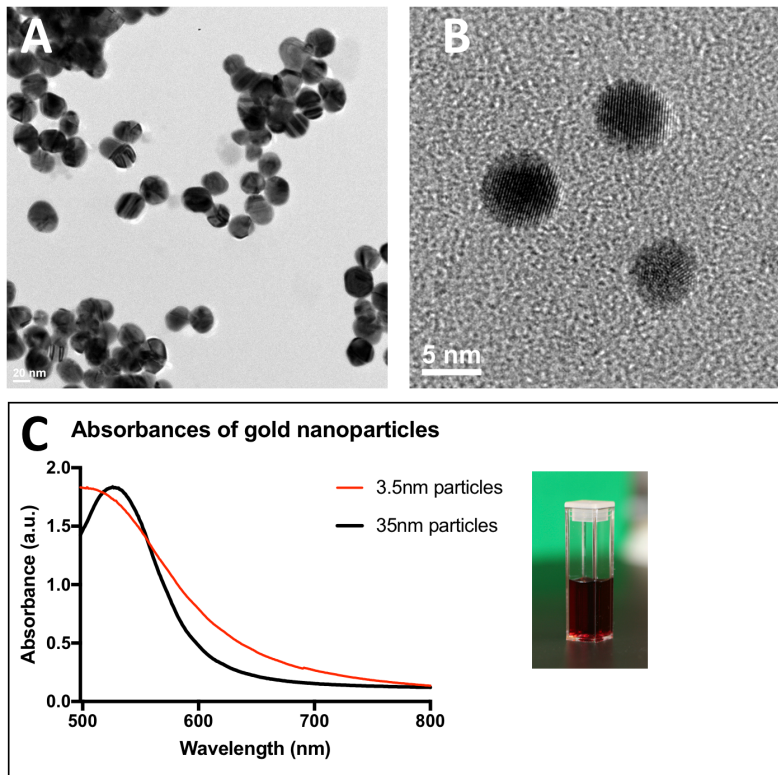


Figure 5.2: A): TEM image of the B-GNP.

B) TEM image of the s-GNP. Note the visible crystalline lattice of the gold with different orientation.

C) comparison between the absorbance spectra of the two type of nanoparticles. As expected, there is the red shift as increasing the dimensions.

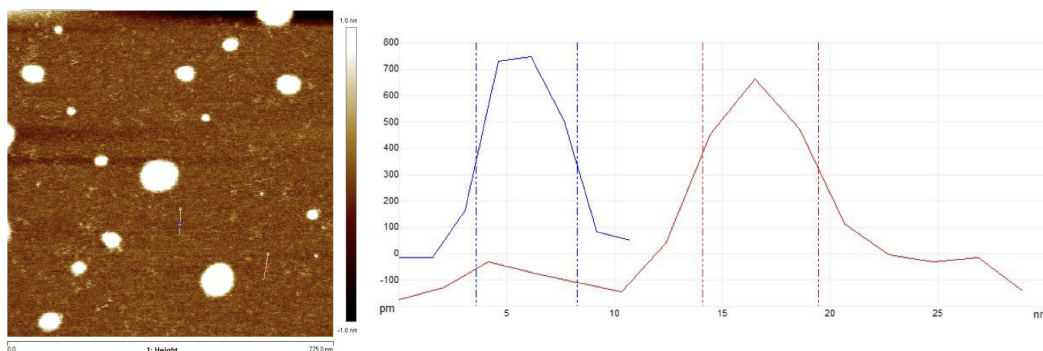


Figure 5.3: On the left: AFM image. On the right: example of image analysis with the AFM software to evaluate the particle diameter.

5.2 *In vitro* experiments results

In this section the results of the *in vitro* experiments will be reported, whose design is explained in chapter 4.1

5.2.1 Evaluation of growth rate of Lewis Lung Cells luciferase expressing

As mentioned in chapter 5.1.1 IVIS images of LLC-Luc in a 96 wells plate were acquired and the ROI were evaluated through the machine's software. In figure 5.4 the acquired images are reported.

As can be seen in figure 5.5 the results are very good and the ROIs show, as expected, an increasing trend. This increasing of luminescence with the increasing of the number of cells during time, proves that the expression of the luciferase persists also in subsequent generations making the LLC-Luc suitable for *in ovo* and *in vivo* experiments.

5.2.2 Cellular uptake experiment

The acquired TEM images are reported in figure 5.6. It is clear that the cells actually internalize the particles, that appear as black spots in the images. However, they enter in the cells in big cluster and this can decrease the radioenhancement effect of GNP. The

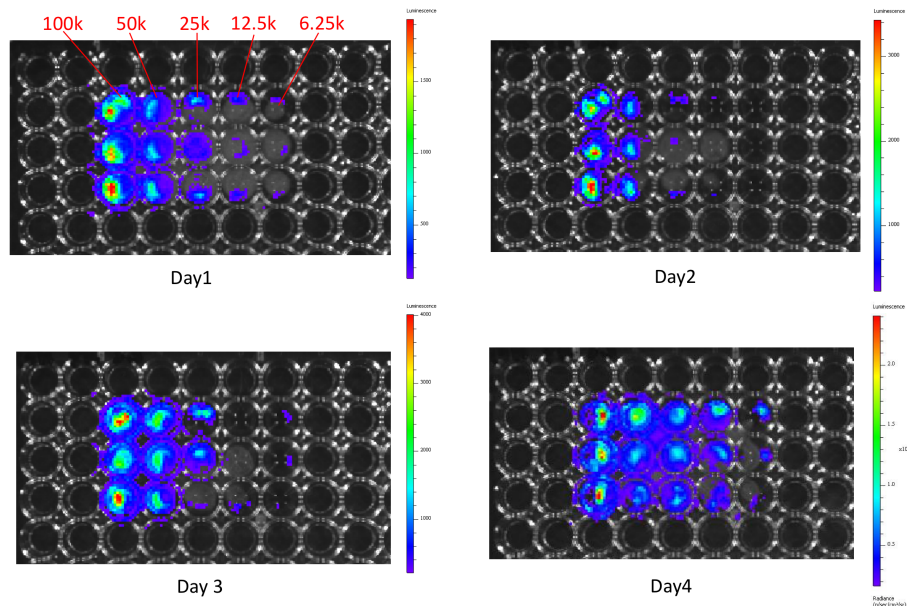


Figure 5.4: IVIS images of LLC-Luc in 96 well plates in 4 different days. Along the columns there are all the different number of cells. Along the rows there are the three samples for each group.

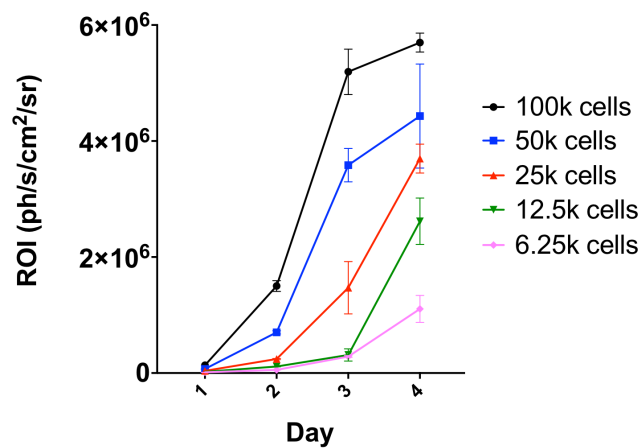


Figure 5.5: ROIs behavior during time and for different starting cells number (LLC-Luc), derived from the post-processing of IVIS images. All the groups show an increasing trend of the ROI during time. Furthermore, the higher the initial number of cells, the higher the ROI value.

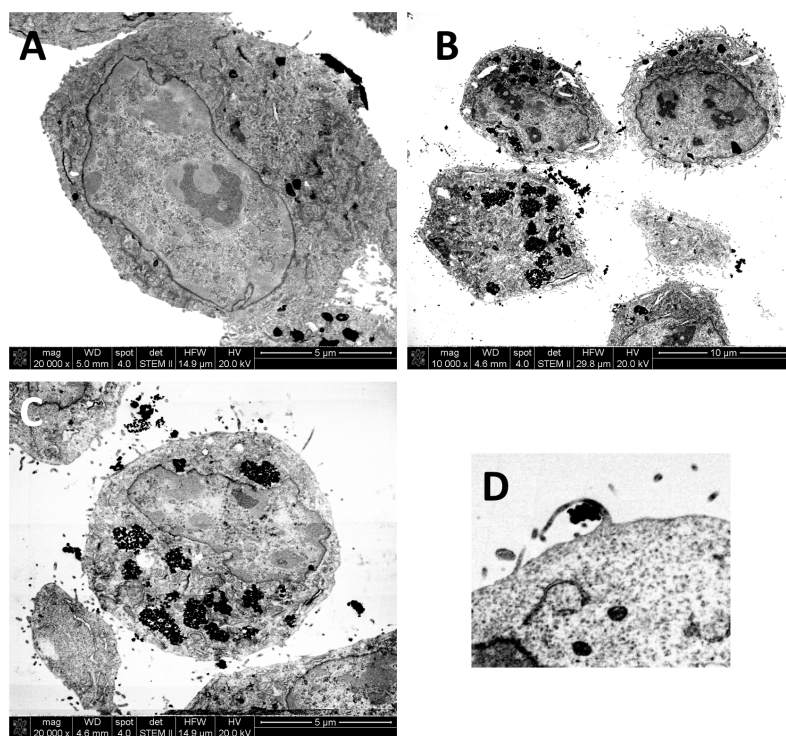


Figure 5.6: TEM images of LLC with internalized GNP, that appear as black spots. The images show the successful cellular uptake, but also the tendency of GNP to form clusters. In (D) a magnification probably shows the moment right before the internalization.

magnification of figure 5.6 (D) is very interesting and probably shows the moment right before the internalization.

5.2.3 Comet assay and clonogenic assay

The result of comet assay is reported in figure 5.7 and the one of clonogenic assay in figure 5.8.

Comet assay result Referring to figure 5.7, on the left the characteristic "comet" images of the four groups involved in the experiments can be seen. On the right the tail moment is represented. Remember that the higher the value, the more the DNA damage due to radiation. Each point corresponds to a cell, while the horizontal line to the mean value. As can be seen there is significance (two stars) between radiation alone and radiation plus nanoparticles, confirming the efficacy of GNP as radioenhancers.

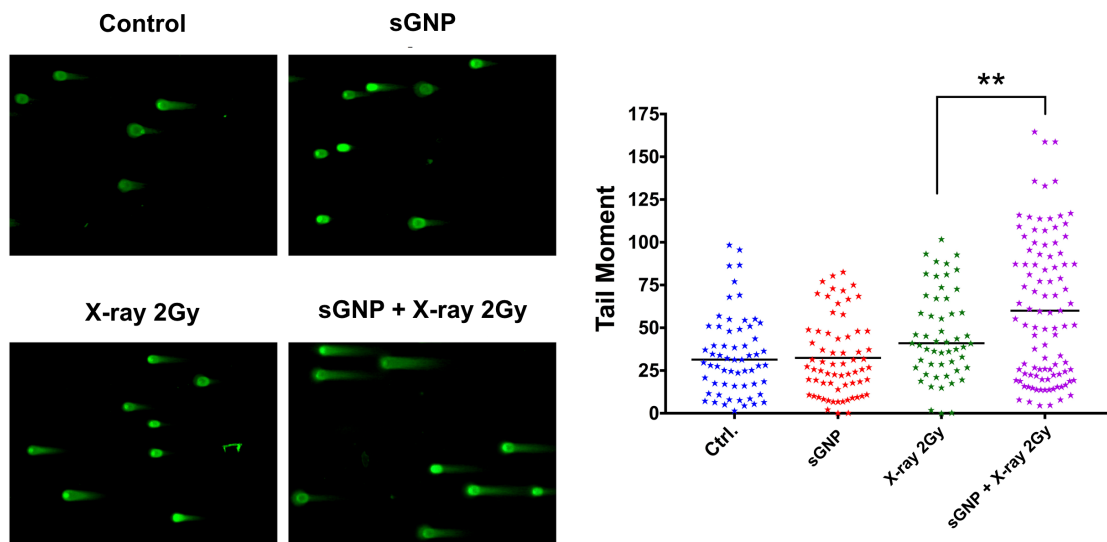


Figure 5.7: Comet assay results: on the left the images where can be noticed the longer tails when sGNP are present with respect radiation alone. On the right the graphical representation of the results: the horizontal bars correspond to the mean value of the points.

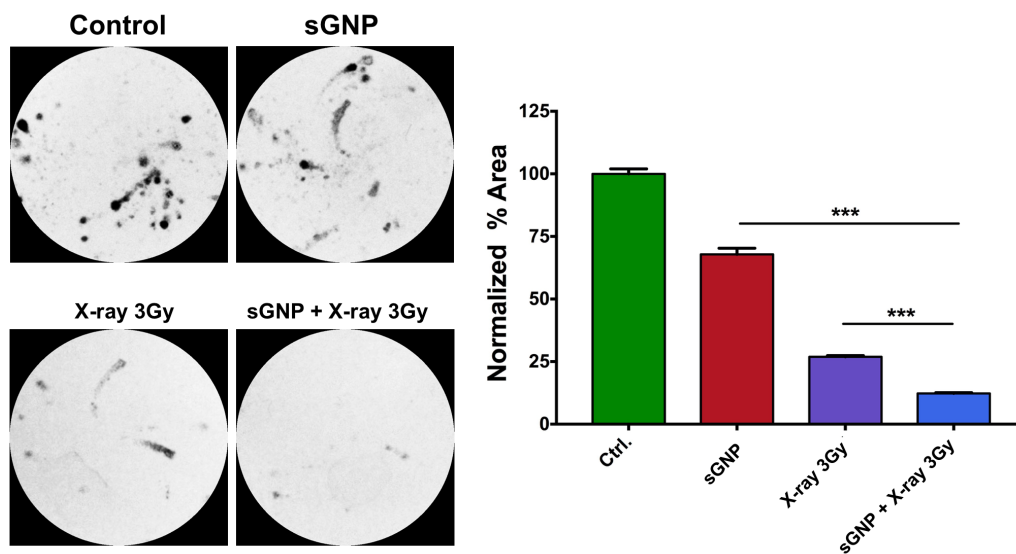


Figure 5.8: Clonogenic assay results: on the left pictures of the colonies in the Petri dishes. On the right the graphical representation of the results expressed in normalized covered area.

Clonogenic assay result Referring to figure 5.8 on the left it can be seen a picture of the cell colonies in the Petri dishes. Unfortunately this assay is very sensitive to the attachment grade of the cells on the surface. As reported in section 3.2, the LLC are for their nature loosely attached. Probably this is the cause of the poor resolution of the image. On the right, the bar graph represents the normalized percentage area covered by the cells, that, for the untreated group (control) results to be 100% with a low standard deviation. We would expected a 100% value also for sGNP alone and this is not verified. This because sGNP have a proved minimal toxicity that, however, is acceptable for biocompatibility. Another reason can be that the particles not always have been conserved under protected atmosphere and in sterile conditions. In presence of radiation, the coverage area reduces more than a half with respect the sGNP alone. And further decreases when particles are added to radiation. As demonstrated by the three stars there is a good significance in the results. The software used for these statistical analysis is *Prysm*[®].

Overall the results of the *in vitro* experiments are satisfying and significant and confirm the radioenhancement capability of sGNP. Furthermore two different radiation doses were tried (2 Gy and 3 Gy) and both present an effect on murine Lewis Lung Cells.

5.3 *In ovo* experiments results

In this section the results of *in ovo* experiments reported in chapter 4.2 will be reported starting from the preliminary ones.

5.3.1 Preliminary experiment: optimization of the initial number of cell

Some pictures of the tumors before harvesting were taken in order to see by eye which one resulted the best. The pictures are reported in figure 5.9.

It is important to notice that all the three groups have tumors, but the ones in figure (B) (1 million) present a more 3D shape with respect the others. In figure (A) we have mostly a "sheet" shape that, however has a certain thickness. The third egg in figure (C) is not healthy and we can say that by looking at the egg color: more opaque and yellowish. The tumors were also measured starting from the pictures in figure 5.9 by using *Matlab*[®]. The average maximum dimension resulted to be (3.02 ± 0.77) mm

After all the considerations, from the first visual inspection, it can be said that the best initial number of cells is 1 million. This is confirmed also by the histological analysis done with H&E staining. In figure 5.10 (A) it is reported a 4x image representing all the collected tissue of the second egg of image 5.9 (B). This is a very nice image that highlights

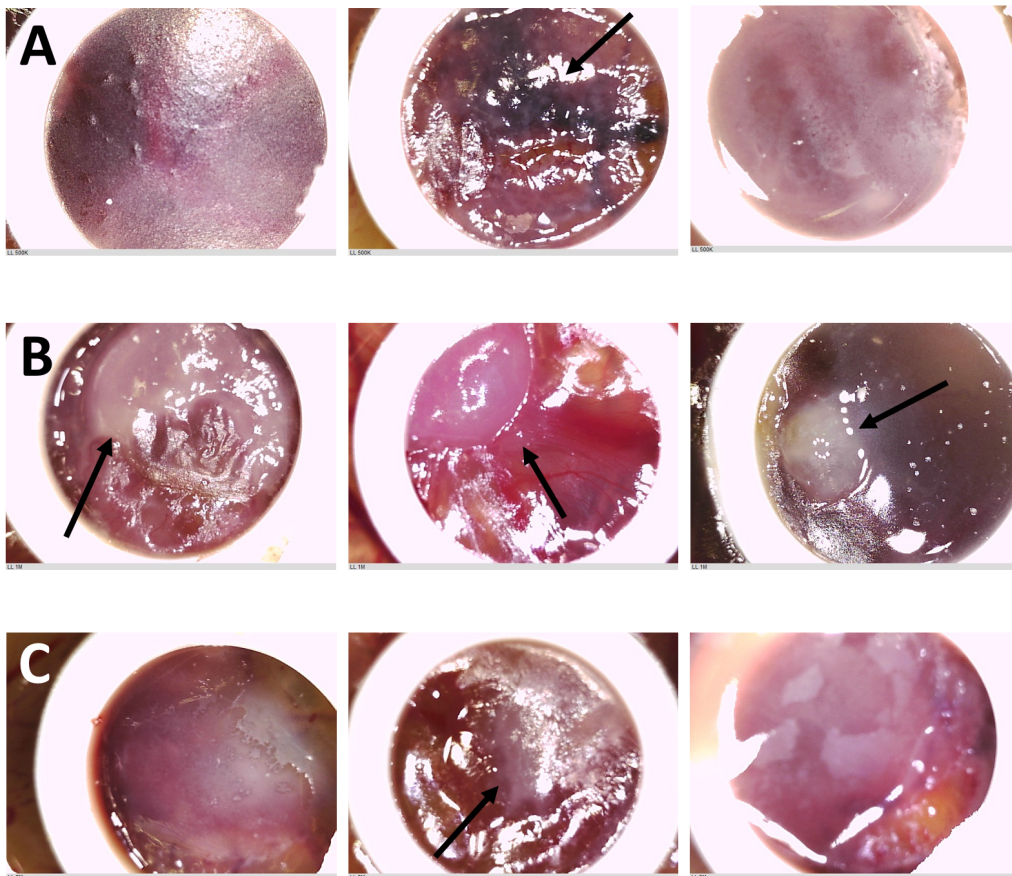


Figure 5.9: Pictures of LLC (passage 5) derived tumors on CAM after 3 days of incubation starting from three different initial number of cells: (A): 0.5 million; (B): 1 million; (C): 2 millions. The arrows indicate the tumors.

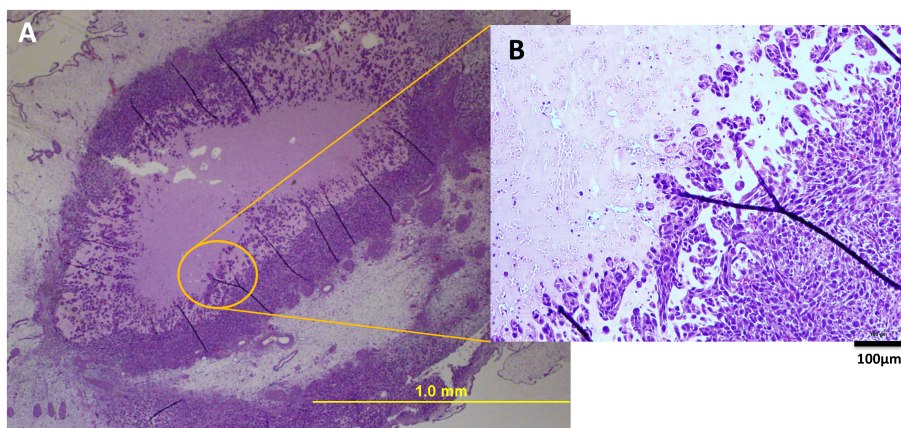


Figure 5.10: H&E images of a LLC derived tumor starting from 1 million cells on CAM. (A): 4x image representing the whole tissue (taken with an *Olympus IX2-UCB*). (B) 10x magnification of the boundary between the living and apoptotic part of the tumor (taken with an *Olympus BX UCB*)

the aggressiveness of the tumor. In fact the dark violet parts indicate the proliferating LLC cells that surround the central part of the nodule that has a lighter and more uniform violet. This is the apoptotic central part, characteristic of cancers. The death of the cells in this part indicate an aberrant growth of the tumor, such that the vessels don't have enough time to reach the inner core of the cancer, that dies. In figure 5.10 (B) a magnification underlines the boundary between this two regions.

5.3.2 Preliminary experiment: optimization of the amount of gold in the eggs and GNP detection

Some pictures of the tumors before harvesting were taken in order to see by eye which one resulted the best. They are reported in figure 5.11.

Note that all the pictures are characterized by a darker region in the center of the silicone ring. These probably are the nanoparticles. All the eggs in picture 5.11 (C) (highest GNP volume) are death proving that this amount of gold is too high. On the other hand (A) and (B) appear good. In particular the third egg in (A) shows also tumor tissue outside the ring, as if a sort of methastasis developed. In fact it can happen that some cells enter in the circulatory system of the egg, bringing them outside the ring. It would be very interesting demonstrating the presence of GNP also in the methastasis, proving the capability of the particles to "follow" the cells, becoming effective, in a radiation treatment, also for methastasis.

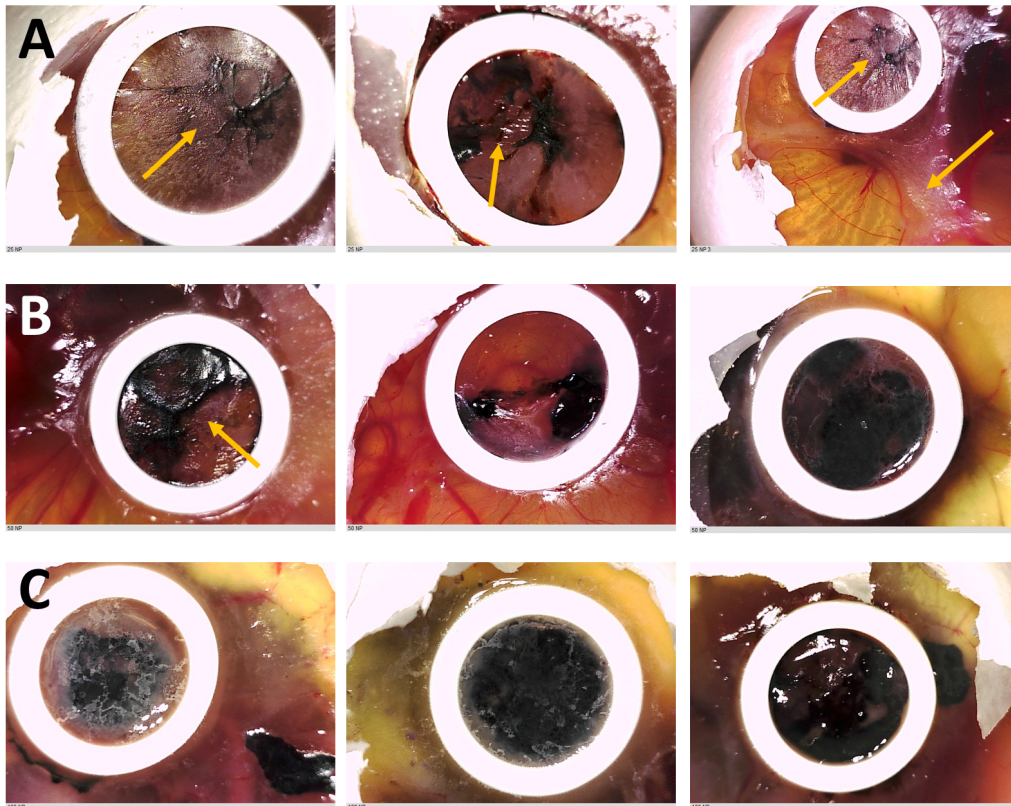


Figure 5.11: Pictures of LLC (passage 8) derived tumors on CAM after 3 days of incubation starting from 1 million cells and three different GNP volumes: (A): 25 μL ; (B): 50 μL ; (C): 100 μL ;

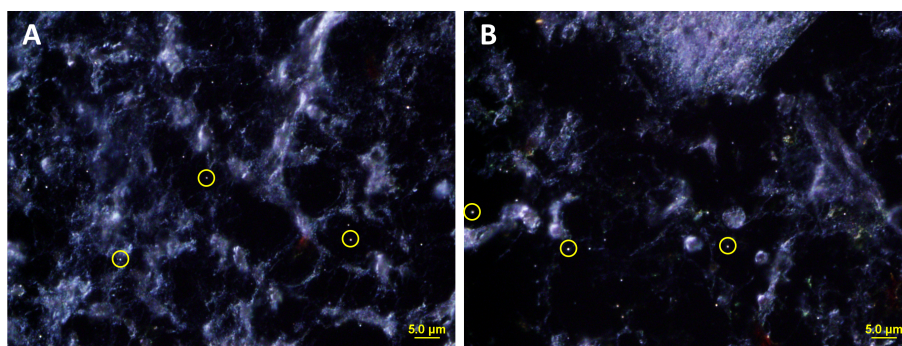


Figure 5.12: Dark field images (oil objective mag. 100x) of silver stained tissues from sample with 25 μL of GNP. (A) and (B) represent two different regions of the same slide. The yellow circles allow a better detection of the particles.

After this considerations we can state that 100 μL of GNP can not be accepted.

Detection of gold nanoparticles with optical microscopy

Thanks to the silver stain used in the histological samples, we were able to detect GNP embedded in the collected tissue. We used dark field microscopy with oil objective.

In figure 5.12 two images are reported. They refer to two different region of the same slide and the sample is the one containing 25 μL of GNP. Note that the particles are perfectly visible and they appear as silvery points in the images. However it is nearly impossible to say if they are embedded in the tumor tissue or in the chicken one, and if they are inside the single cell or not. In order to examine in depth this point, we tried to counter stain the slides with standard H&E staining maintaining the dark field type of microscopy, but the results, reported in figure 5.13, are still not satisfying. The problem with optical microscopy with 100x magnification is that you don't really know where you are along the slide. One should scan systematically the whole slide, but at this point a more sophisticated equipment is needed with a stepper that automatically moves the slide below the objective and acquires images. A microscope like this was present in the "imaging suite" of the Houston Methodist Research Institute but it was not possible to perform dark field images with a so high magnification. Furthermore the stitching process of the acquired images requires too much time.

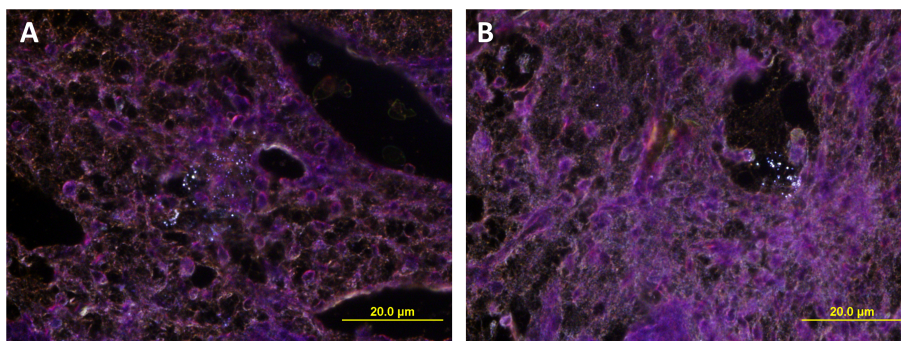


Figure 5.13: Dark field images (oil objective mag. 100x) of silver stained tissues with H&E counter staining from sample with 25 μL of GNP. (A) and (B) represent two different regions of the same slide.

5.3.3 Preliminary experiment: optimization of the X-ray dose for the eggs

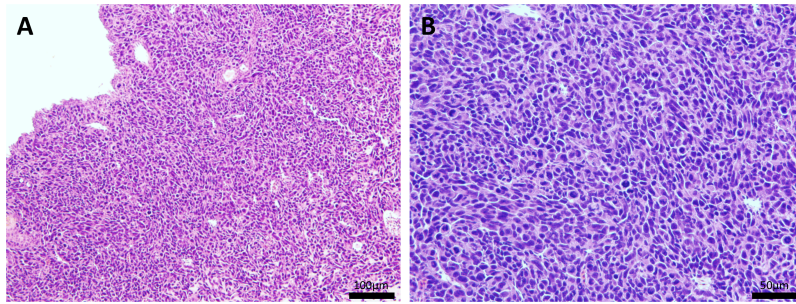
In figure 5.14 the most significant histological results are reported for each group. First of all the untreated group results healthy and the tumor cells are well packed. Although in 5.14(b) there is not a visible tissue damage, in 5.14(c), 5.15(a) and 5.15(b) for sure there are regions in which cells are dead. The effect can be easily attributed to radiation since the apoptotic region is not in the center of the nodule (as in figure 5.10 of chapter 5.2.1) but is distributed in a uniform way along the whole tumor. On the other hand (c) shows an excessive effect of the radiation: 4 Gy can not be used for the future experiments with GNP. In fact it would be difficult to estimate a further damage since the tumor cells in this case have been almost totally killed. The dose 2 Gy + 2 Gy results to be the best trade off and in figure 5.15(a) it is reported the clear boundary between damaged part and still alive tumor cells.

In table 5.1 it is reported a summary of the results for the *in ovo* preliminary experiments.

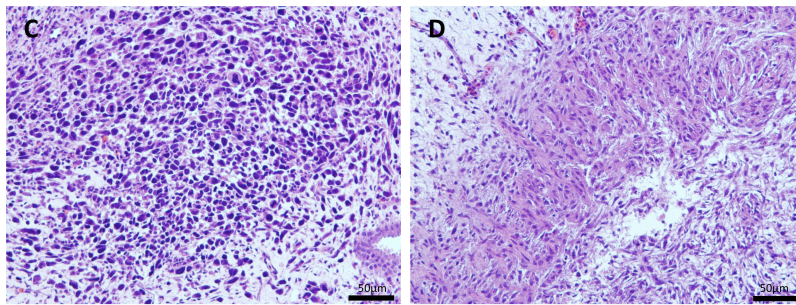
5.3.4 Synergistic effect of gold nanoparticles and radiation

In figures 5.16, 5.17 and 5.18 the IVIS images of one egg per group are reported. Each panel corresponds to the evolution in time of the signal (from Day 1 to Day 4). It is also underlined the ROI evaluation in the imaging post processing.

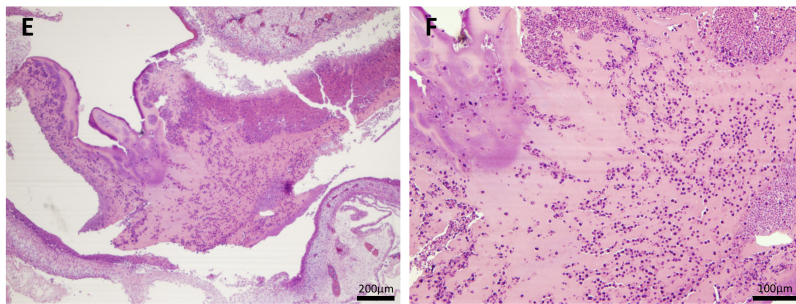
In figure 5.19, instead, the results are represented in a graphical way, summarizing the behavior of all the eggs. The n is also reported, i.e. the number of eggs considered. Note



(a) Controls



(b) Radiation dose: 2 Gy



(c) Radiation dose: 4 Gy

Figure 5.14: Histological samples from the different groups of radiation optimization experiment of eggs. Here the control and the single dose groups are reported

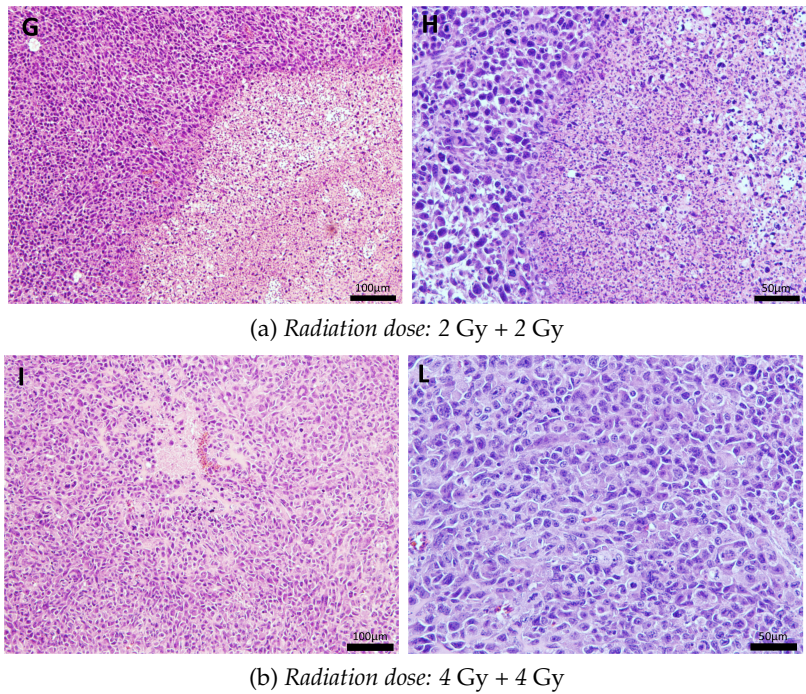


Figure 5.15: Histological samples from the different groups of radiation optimization experiment of eggs. Here the groups with fractionated doses are reported. 2 Gy + 2 Gy results to be the best solution

Table 5.1: Summary of the *in ovo* preliminary experiments results

Investigated quantity	Tried groups	Best solution
Initial number of cells	500K 1M 2M	1M
Amount of gold per egg	25 µL 50 µL 100 µL	(25÷50) µL
X-ray dose	2 Gy 4 Gy (2+2) Gy (4+4) Gy	(2+2) Gy

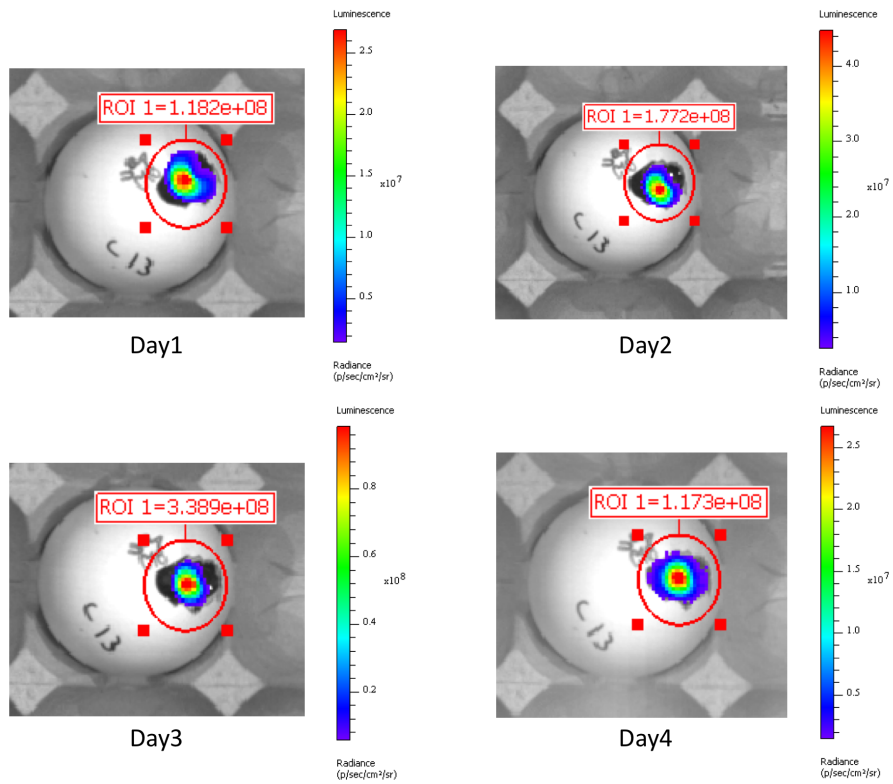


Figure 5.16: IVIS images of one untreated egg during time

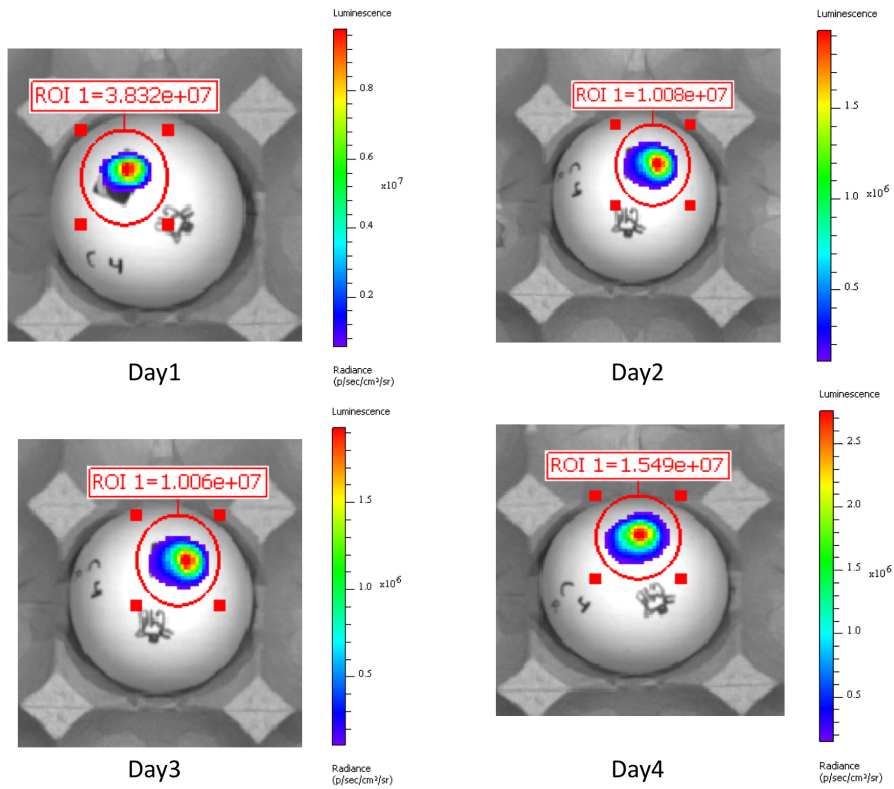


Figure 5.17: IVIS images during time of one egg subjected to radiation only

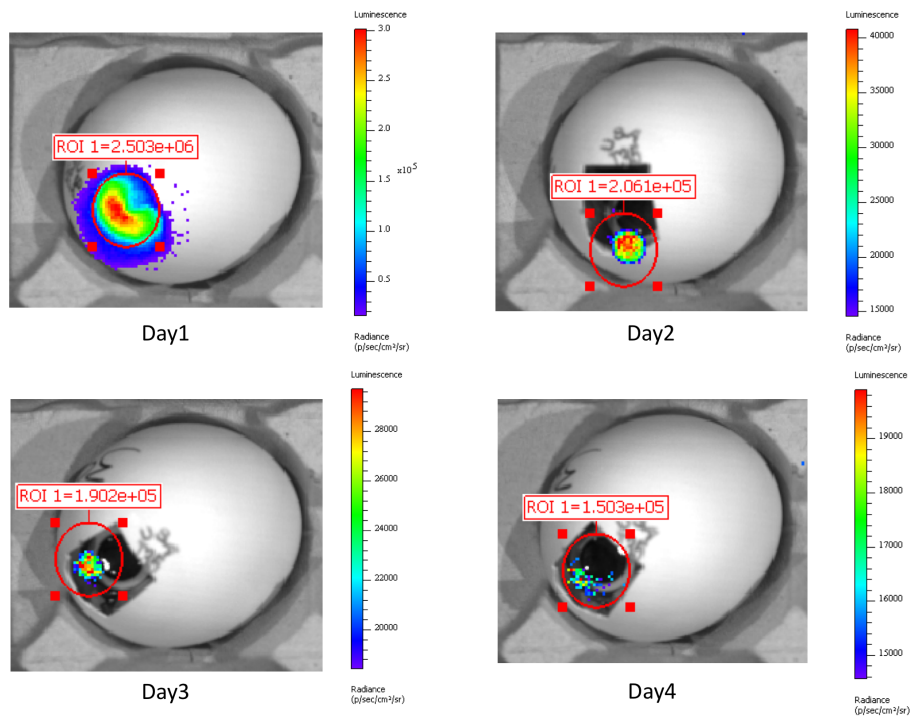


Figure 5.18: IVIS images during time of one egg subjected to radiation + GNP effect

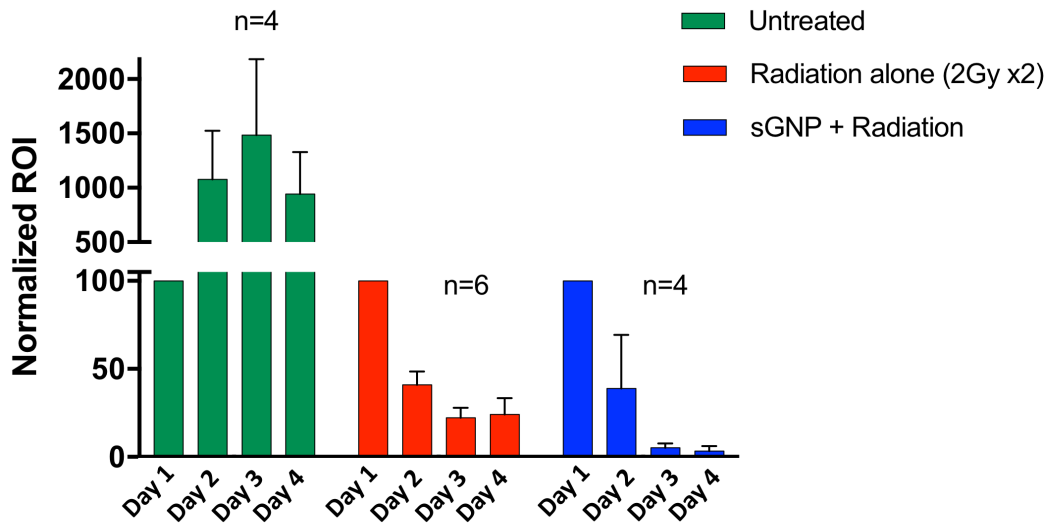


Figure 5.19: Normalized ROIs from IVIS images of the eggs during radiation treatment. The difference between radiation alone and GNP + radiation is significant and demonstrate the radioenhancement effect of gold nanoparticles.

that just the living eggs were taking into account in order to not distort the results. At the beginning, in fact, the eggs were 6 per group, but few died during the experiment. In the graph the normalized ROI is reported to facilitate the data understanding. This means that we measured the ROI for each egg, did the average between eggs of the same group for each day and finally normalized the data to the first day, giving a starting value of a representative "100" to easily see the behavior for the subsequent days. That's why in the first day there is not present any standard deviation.

The results are very satisfying and we can notice a significant difference between the effect of radiation alone with respect radiation + GNP especially from day 3 where the signal of the irradiated group is still high than the one with GNP.

Overall we can say we have proven the radioenhancement ability of gold nanoparticles *in ovo*.

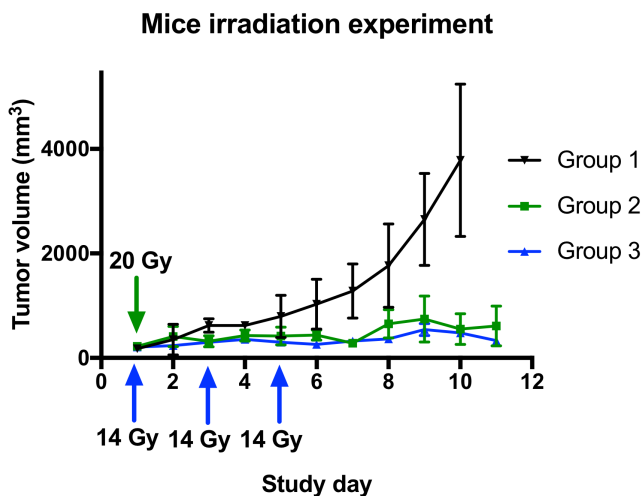


Figure 5.20: Volume measurements of LLC derived tumors in mice treated with radiation. The arrows indicate the irradiation sessions and the doses. The group 1 is the untreated group; group 2 was treated with a single 20 Gy dose; group 3 with three doses of 14 Gy each. Note that both group 2 and group 3 present a significant decreasing in tumor growing with respect the control group.

5.4 *In vivo* experiments results

5.4.1 Preliminary experiment: optimization of radiation dose

As explained in chapter 4.3.1, the tumor volume was taken as significant parameter to monitor the tumor growth in mice and the measurements were taken every day. The result is reported in figure 5.20. The black line represents the control group, i.e. the mice that did not receive radiations, the blue line represents the group that received three radiation doses of 14 Gy each and the green line the group that received only one dose of 20 Gy. The graph shows the stop of tumors growth for both the irradiated groups, suggesting a too much high radiation effect, not suitable for the future GNP radioenhancement effect experiments. The irradiated mice were euthanized after 11 days from the first irradiation while the control mice were euthanized after 10 days.

Overall, the results of this first *in vivo* experiment is satisfying, but suggests to lower the doses for the next experiments with GNP.

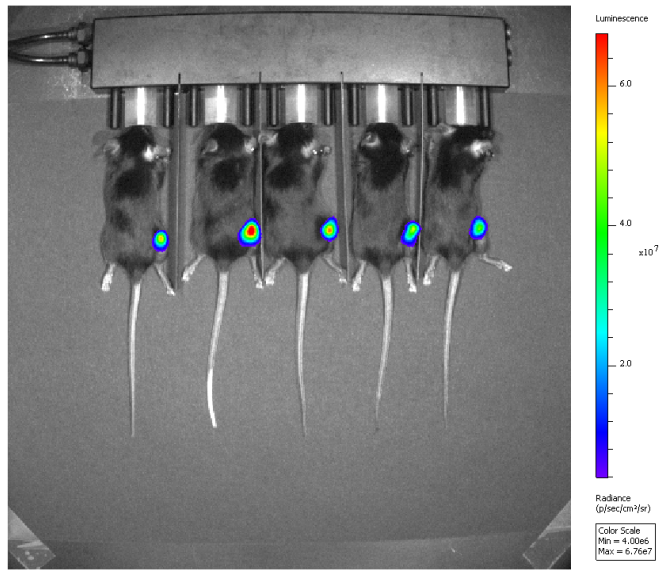
5.4.2 *In vivo* GNP radioenhancement

We took IVIS images for 4 days during radiation treatment after which all the mice were sacrificed. The tumors were collected together with the spleens for future experiments to evaluate the biodistribution through ICP-MS. Some tumors were frozen in liquid nitrogen (for ICP-MS), some other fixed for histology.

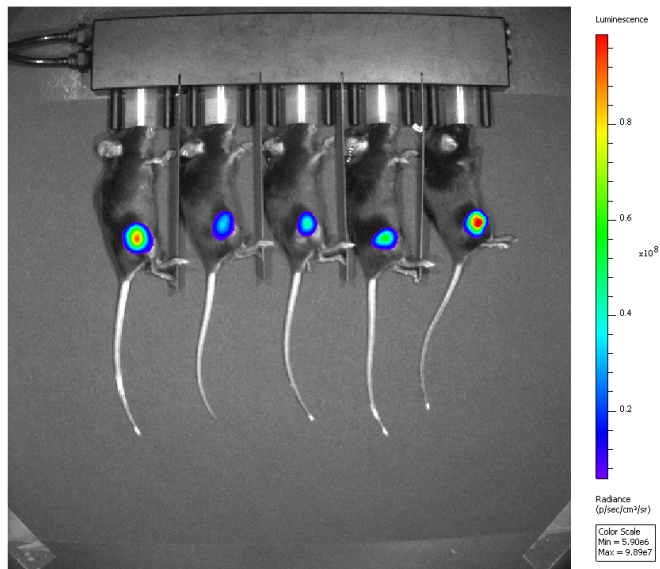
Not all the images will be reported. An example can be seen in figure 5.21 where it can be noticed that we tried more than one mice positioning. The best one is with the mice on one side. The acquired images were processed and the ROI evaluated. In figure 5.22 the normalized ROI is reported. Note that for each group the n is equal to 5. In fact, just the best five mice (over 8) are here considered. On the contrary of the eggs, here the GNP effect is not clear nor consistent for both the radiation types. This can be due to several factors. One among all the gold amount. In literature there are several mice experiment in which the gold solution injected has a very high concentration (up to 10 times the one we used). However for us it was very difficult to reach this concentration with traditional centrifuge and to still not clog the needle. Furthermore it has to be taken into account that from the IACUC protocol there is a maximum volume that can be injected intratumorally. These factors made the achieving of such high amount of gold impossible for us.

Another reason can be the type of injection. Remember that in the eggs the GNP were inoculated well dispersed together with the cells allowing an homogeneous distribution in the tumor. The intratumoral injection unavoidably localizes the particles in just one point, preventing the optimal GNP action.

Moreover the radiation dose is not yet well established so it is better to further optimize it for future experiments.



(a)



(b)

Figure 5.21: Example of IVIS image of the mice with the two different positioning. Although tumors are visible in both images, the best mice position is on one side as in (b).

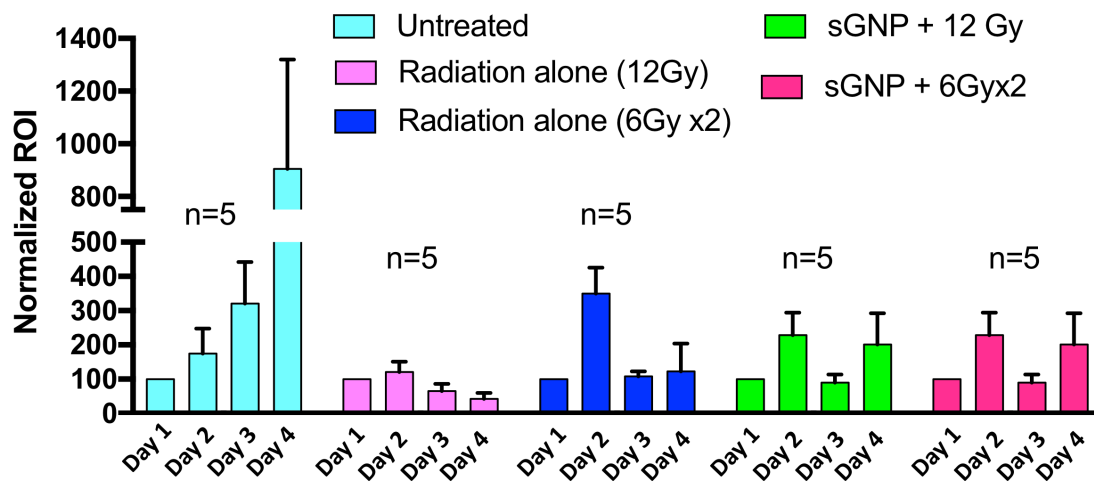


Figure 5.22: Normalized ROIs from IVIS images of mice. It is not clear the difference between radiation alone and radiation + GNP. On the other hand the control group presents the expected behavior.

Chapter 6

Conclusions, improvements and future work

In this study we successfully demonstrated how the CAM model can be used for radiotherapy experiments and we proved the GNP radiation enhancement effect in both *in vitro* and *in ovo* models. We successfully inoculated LLC and GNP on CAM and, for the first time, we irradiated the eggs obtaining very good outcomes suitable as preliminary data for further future experiments. We experimented the several advantages of the CAM: from the costs to the speed of the experiments. Unfortunately one disadvantage of the CAM is its fragility. During all the *in ovo* experiments we moved the eggs from one lab to the other in order to perform radiation and imaging. Of course this represents a stress for the eggs that led several times to the death of the embryo causing difficulties during experiments that had to be repeated.

Unfortunately we had not the expected results with the *in vivo* experiment.

Several are the possible improvements that can be applied at this study. I will schematically list some ideas:

For *in ovo* experiments:

Due to the fragility of the eggs all the equipments must be in the same place to avoid stress to the eggs that can bring to death.

For *in vivo* experiments:

1. A further optimization of radiation doses is needed

2. To avoid the localization of GNP, multiple injections can be performed along the tumor and wait some time to allow the distribution before irradiation
3. The concentration of the GNP has to be increased

Diagnostic tools:

For both the *in ovo* and *in vivo* work, we exploit the IVIS imaging as diagnostic tool to monitor tumor growing. However it is not fully quantitative. It is necessary to investigate other techniques such as PET or CT imaging, or in any case, a tool that allows a 3D image elaboration in order to unequivocally measure the tumor volume and monitor its dimension during treatments.

More experiment are nowadays in progress at the Houston Methodist Research Institute that are investigating all these aspects. Furthermore it would be interesting doing a biodistribution study of the unfunctionalized GNP and taking in consideration the possibility to stabilize the colloidal with PEG to avoid coagulation as demonstrated in chapter 4.1.2. Another very interesting aspect is the study of the difference among the effects of the sGNP with respect the BGNP. This requires a lot of time and again the performing of all the optimization experiments.

Overall I am very satisfied of all the work I have done. In these few months I had the possibility to work with brilliant scientists and to learn a lot, filling the gaps of my knowledge by putting the hands on biology and animal studies.

Bibliography

- [1] Siegel R. L., Miller K. D., and Jemal A. Cancer statistics, 2017. *CA: A Cancer Journal for Clinicians*, 2017.
- [2] Shrestha S., Cooper L. N., Andreev O. A., Reshetnyak Y. K., and Antosh M. P. Gold nanoparticles for radiation enhancement n vivo. *Jacobs Journal of Radiation Oncology*, 3(1):026, 2016.
- [3] Sonavane G., Tomoda K., and Makino K. Biodistribution of colloidal gold nanoparticles after intravenous administration: effect of particle size. *Elsevier - Colloids and Surfaces*, 66(2):274–278, 2008.
- [4] Chithrani D. B, Jelveh S., Jalali F., van Prooijen M., Allen C., Bristow R. G., Hillc R. P., and Jaffray D. A. Gold nanoparticles as radiation sensitizers in cancer therapy. *Radiation Research*, 173(6):719–728, 2010.
- [5] Li M., Pathak R. R., Lopez-Rivera E., Friedman S. L., Aguirre-Ghiso J. A., and A. G. Sikora. The in ovo chick chorioallantoic membrane (CAM) assay as an efficient xenograft model of hepatocellular carcinoma. *Journal of Visualized Experiments*, 104:e52411, 2015.
- [6] Deryugina E. I. and Quigley J. P. Chick embryo chorioallantoic membrane model systems to study and visualize human tumor cell metastasis. *Histochemistry and Cell Biology*, 130(6):1119–1130, 2008.
- [7] Moreno-Jimenez I., Hulsart-Billstrom G., Lanham S. A., Janeczek A. A., Kontouli N., Kanczler J. M., Evans N. D., and Oreffo R. O. The chorioallantoic membrane (CAM) assay for the study of human bone regeneration: a refinement animal model for tissue engineering. *Nature Scientific Reports*, 6:32168, 2016.
- [8] McQuaid H. N., Muir M. F., Taggart L. E., Coulter J. A. McMahon S.J, Hyland W. B., Jain S., Butterworth K. T., Schettino G., Prise K. M., Hirst D. G., Botchway S. W., and Currell F. J. Imaging and radiation effects of gold nanoparticles in tumour cells. *Nature Scientific Reports*, 6:19442 EP, 2016.

- [9] Hoo C. M., Starostin N., West P., and Mecartney M. L. A comparison of atomic force microscopy (AFM) and dynamic light scattering (DLS) methods to characterize nanoparticle size distributions. *Journal of Nanoparticle Research*, 10:89–96, 2008.
- [10] Hunter R.J., Ottewill R.H., and Rowell R.L. Zeta potential in colloid science: principles and applications. "Academic press" Publisher.
- [11] Haiss W., Thanh N. T. K., Aveyard J., and D. G. Fernig. Determination of size and concentration of gold nanoparticles from UV-Vis spectra. *Analytical chemistry*, 79:4215–4221, 2007.
- [12] Bertram J.S. and Janik P. Establishment of a cloned line of lewis lung carcinoma cells adapted to cell culture. *Cancer letters*, 11:63–73, 1980.
- [13] Goda K., Hatta-Ohashi Y., Akiyoshi R., Sugiyama T., Sakai I., Takahashi T., and Suzuki H. Combining fluorescence and bioluminescence microscopy. *Microscopy Research and Technique*, 78(8):715–722, 2015.
- [14] Wilson K., Yu J., Lee A., and Wu J.C. In vitro and in vivo bioluminescence reporter gene imaging of human embryonic stem cells. *Journal of Visualized Experiments*, 14:740, 2008.
- [15] Hastings J.W. Chemistries and colors of bioluminescent reactions: a review. *Gene*, 173:5–11, 1996.
- [16] Anonymous. Electron microscopy procedure manual. *Fred Hutchinson Cancer Research Center*, 2010.
- [17] Nandhakumar S., Parasuraman S., Shanmugam M.M., Ramachandra Rao K., Chand P., and Vishnu Bha B. Evaluation of DNA damage using single-cell gel electrophoresis (comet assay). *Journal of pharmacology and pharmacotherapeutics*, 2(2):107–111, 2011.
- [18] Guzma C., Bagga M., Kaur A., Westermarck J., and Abankwa D. Colony area: An ImageJ plugin to automatically quantify colony formation in clonogenic assays. *PLoS ONE*, 9(3):e92444, 2014.
- [19] Munshi A., Hobbs M., and Meyn R.E. Clonogenic cell survival assay. *Methods in Molecular Medicine*, 110:21–28, 2005.
- [20] Boisselier E. and Astruc D. Gold nanoparticles in nanomedicine: preparations, imaging, diagnostics, therapies and toxicity. *Chemical Society Reviews*, 38(6):1759–1782, 2009.
- [21] Alkilany A. M. and Murphy C. J. Toxicity and cellular uptake of gold nanoparticles: what we have learned so far? *Journal of Nanoparticle Research*, 12(7):2313–2333, 2010.

- [22] Yao X., Huang C., Chen X., Yi Z., and Sanche L. Chemical radiosensitivity of DNA induced by gold nanoparticles. *Journal of Biomedical Nanotechnology*, 11(3):478–485, 2015.
- [23] Hainfeld J. F., Slatkin D. N., and Smilowitz H. M. The use of gold nanoparticles to enhance radiotherapy in mice. *Physics in Medicine and Biology*, 49:N309–N315, 2004.
- [24] Chen J., Shen Z., Zheng Y., Wang S., and Mao W. Radiotherapy induced lewis lung cancer cell apoptosis via inactivating β -catenin mediated by upregulated HOTAIR. *International Journal of Clinical and Experimental Pathology*, 8(7):7878–7886, 2015.